

# **JGR Space Physics**

# <del>L</del>

#### RESEARCH ARTICLE

10.1029/2024JA032933

#### **Key Points:**

- 2021 Hurricane Grace's impact on electron density, thermospheric winds, and temperature are analyzed using COSMIC-2, ICON, and GOLD
- Ionospheric electron density showed notable variations, predominantly increasing with the hurricane's intensification
- Significant thermospheric warming and circulation changes are observed

#### Correspondence to:

E. Yiğit, eyigit@gmu.edu

#### Citation

Gann, A. L. S., & Yiğit, E. (2024). Ionospheric and thermospheric effects of Hurricane Grace in 2021 observed by satellites. *Journal of Geophysical Research: Space Physics, 129*, e2024JA032933. https://doi.org/10.1029/2024JA032933

Received 31 MAY 2024 Accepted 2 OCT 2024

#### **Author Contributions:**

**Conceptualization:** Ayden L. S. Gann, Erdal Yiğit

Data curation: Ayden L. S. Gann Formal analysis: Ayden L. S. Gann, Erdal Yiğit

Funding acquisition: Erdal Yiğit Investigation: Ayden L. S. Gann, Erdal Yiğit

Methodology: Ayden L. S. Gann, Erdal Yiğit

**Project administration:** Erdal Yiğit **Resources:** Erdal Yiğit

**Software:** Ayden L. S. Gann, Erdal Yiğit **Supervision:** Erdal Yiğit

Validation: Ayden L. S. Gann, Erdal Yiğit Visualization: Ayden L. S. Gann, Erdal Yiğit

Writing – original draft: Ayden L. S. Gann, Erdal Yiğit Writing – review & editing: Ayden

Writing – review & editing: Ayden L. S. Gann, Erdal Yiğit

© 2024 The Author(s).

This is an open access article under the terms of the Creative Commons

Attribution-NonCommercial License, which permits use, distribution and reproduction in any medium, provided the original work is properly cited and is not used for commercial purposes.

# **Ionospheric and Thermospheric Effects of Hurricane Grace** in 2021 Observed by Satellites

Ayden L. S. Gann<sup>1</sup> and Erdal Yiğit<sup>1,2</sup>

<sup>1</sup>Department of Physics and Astronomy, Space Weather Lab, George Mason University, Fairfax, VA, USA, <sup>2</sup>Goddard Space Flight Center, NASA GSFC, Greenbelt, MD, USA

**Abstract** Effects of Hurricane Grace in August 2021 are studied in the thermosphere and ionosphere, using data from the COSMIC-2, ICON, and GOLD satellites. Significant impacts on electron density, thermospheric winds, and temperature are observed after the onset of the hurricane, compared to the pre-hurricane phase. Comparison of the observations during the hurricane with the ones during a non-hurricane year clearly provides further evidence for substantial hurricane-induced thermospheric and ionospheric changes. We reveal an enhancement in electron density during the hurricane's rapid intensification and pronounced changes in thermospheric winds. Additionally, the low-latitude thermosphere exhibits considerable warming of up to 70 K around 150 km during this period. These changes highlight the long-range vertical coupling mechanisms between hurricanes and the upper atmosphere, and provide valuable insights into the profound influence of meteorological events on upper atmospheric dynamics, emphasizing the need for further exploration.

**Plain Language Summary** Our research investigates how hurricanes, specifically Hurricane Grace in 2021, affect Earth's upper atmosphere. The hurricane was able to influence layers of the atmosphere that are critical for satellite communication and GPS. We used data from different satellites to study changes in the number of free electrons per unit volume of air (electron density), neutral winds, and temperature. We found that during the intensification of the hurricane, electron density increased in the ionosphere, which is the layer of Earth's atmosphere containing a high concentration of ions and free electrons. We also observed substantial changes in the winds high up in the atmosphere and found that a region of the upper atmosphere around 150 km warmed significantly. This research helps us understand how weather events on the Earth's surface can impact conditions hundreds of kilometers above the surface in Earth's atmosphere.

#### 1. Introduction

Hurricanes, representing one of the most potent recurring meteorological events, are key modulators of Earth's temperature by removing excess heat and preventing overheating of the atmosphere and ocean surface layer. These storms are important components of the ocean-atmosphere-ionosphere system. They influence large-scale environmental processes and facilitate interactions between different layers of Earth's environment. On a global scale, tropical cyclones contribute to the transfer of heat, energy, and mass, thereby playing a vital role in maintaining thermal equilibrium in the atmosphere and ocean surface (Chernogor, 2023). They have also been known to generate upward-propagating gravity waves (GWs), with new evidence suggesting outward-radiating spiral gravity waves, confirmed with both aircraft observations and numerical simulations (Nolan & Zhang, 2017). On the other hand, the transfer of energy and momentum by GWs of lower atmospheric origin produce atmospheric vertical coupling over a wide range of spatiotemporal scales (D. C. Fritts & Alexander, 2003; Yiğit, Koucká Knížová, et al., 2016; Yiğit & Medvedev, 2015; Koucká Knížová et al., 2021). During transient meteorological events, such as hurricanes and sudden stratospheric warmings, this coupling is substantially enhanced due primarily to increased internal wave activity, which can be associated with rapid changes in the temperature and circulation of the lower and middle atmosphere (Yiğit & Medvedev, 2016). Hurricanes are strong sources of deep convective activity, which can produce a broad spectrum of short-period GWs (Kuester et al., 2008). Similarly, severe meteorological storms, particularly their frontal systems, can generate gravity waves that propagate upward, causing significant disturbances in both stratospheric and ionospheric parameters (Koucká Knížová et al., 2020). These GWs can propagate from the lower atmosphere to the thermosphere and ionosphere, growing in amplitude and producing long-range coupling (Hickey et al., 2009; Yiğit et al., 2021). In the upper atmosphere, these waves either dissipate or reach saturation due to nonlinear interactions, molecular viscosity, thermal conduction, and ion-neutral friction (Medvedev et al., 2017; Yiğit et al., 2008). Changes in GW

GANN AND YIĞIT 1 of 26

sources in the lower atmosphere may modulate their sources and activity at higher altitudes (Medvedev et al., 2023).

Although ionospheric disturbances triggered by GWs in the presence of hurricanes have been recognized for some time, beginning with Bauer (1958), there is a need to continue to study these effects. The 2020 Atlantic hurricane season, the most active to date (Beven, 2021), emphasizes this need. While there is no consensus on increased storm frequency, the role of climate change in enhancing tropical cyclone intensity is widely recognized (Méndez-Tejeda & Hernández-Ayala, 2023).

Since the discovery of an increase in  $f_0 F_2$  during hurricanes in the 1950's, the field has focused on similar phenomena through both observations and numerical models. More recent studies have indicated hurricaneinduced effects on the upper atmosphere and ionosphere, especially on ionospheric parameters such as the total electron content (TEC) and ionospheric critical frequencies for  $f_0 F_1$  and  $f_0 F_2$  (Ashneel, 2022; Guha et al., 2016; Xu et al., 2019). It has also been demonstrated that atmospheric turbulence and waves generated by tropical cyclones significantly affect ionospheric plasma. Ionospheric perturbations were detected in nearly 65% of Category 5 cyclones, and 50% of Category 4 cyclones; these disturbances often have scales characteristic of acoustic waves and were observed to extend over regions much larger than the storm itself, with electron concentration fluctuations proportional to the cyclone's strength (Zakharov, 2020). Similarly, electromagnetic measurements from SWARM during Typhoon Vonfong (2014) were analyzed and "magnetic ripples" in the upper atmosphere were identified. These quasi-periodic fluctuations produced by the interaction of acoustic waves with the ionosphere indicate the presence of small-scale longitudinal currents (Martines-Bedenko et al., 2019). Additionally, it was found that TEC and critical frequency perturbations can reach two standard deviations during meteorological storms, with increased acoustic-gravity wave generation in the lower atmosphere being a key factor (Borchevkina et al., 2020). Significant wave-like TEC disturbances during tropical cyclones have been noted (Polyakova & Perevalova, 2011). These disturbances can lead to anomalous decreases in TEC, as observed during the active stage of tropical cyclones (Guha et al., 2016).

Advances in numerical modeling have allowed detailed studies of hurricanes, primarily focusing on lower atmospheric and oceanic processes. Recent studies with numerical models have spotlighted influences of sea surface temperature, ocean stratification, and wave conditions on hurricane behavior and coastal impacts, with improved forecasts from assimilating surface fluxes and dropsonde observations, and emphasizing the roles of the ocean mixed layer and aerosols in hurricane dynamics (Cotton & Walko, 2021; Davis et al., 2022; R. Ezer, 2019; Feng & Wang, 2019; Fritts, 2020; J. Li et al., 2020; Zambon et al., 2021). While direct modeling of hurricane effects on the upper atmosphere remains limited, emerging research is exploring how large-scale meteorological systems and convective activity can influence the upper atmosphere and ionosphere. Acoustic and gravity wave interactions above meteorological systems have been modeled, demonstrating how these waves can reach high altitudes and produce observable signatures in the ionosphere (Snively et al., 2022). Also there has been a multimodel approach to investigate how atmospheric waves from tropospheric sources influence thermospheric and ionospheric parameters, revealing effects on Total Electron Content (TEC) and neutral composition (Kurdyaeva et al., 2024). Models have also been used to simulate GW generation and propagation due to hurricanes. It was found that stratospheric GWs can serve as proxies for hurricane intensification, with significant correlations between the two (Wu et al., 2021). Deep convection was identified as a major source of GWs over Hurricane Humberto (Kuester et al., 2008). Furthermore, the impact of sea spray and oceanic eddies on hurricane development was evaluated using a coupled atmosphere-ocean wave modeling system (Bao et al., 2000). Super-inertial internal waves generated by tropical cyclones propagate vertically and laterally, contributing to turbulent mixing and thermocline stratification, with slow, low-latitude storms producing the most significant kinetic energy and vertical velocity responses due to nonlinear advection and vorticity conservation mechanisms (Zedler, 2009).

The availability of high-resolution observational data has advanced the study of hurricane effects on the atmosphere. Enhanced atmospheric motion vectors (AMVs) from geostationary satellites have significantly improved hurricane forecasts by providing crucial dynamical information on storm evolution and landfall impacts (J. Li et al., 2020; Stettner et al., 2019). Similarly, the assimilation of upper-level dropsonde observations has been shown to improve the accuracy of hurricane analyses and intensity forecasts (Feng & Wang, 2019). The development of the Tropical Cyclones Information System (TCIS) has further facilitated the integration of multiparameter satellite and airborne observations, enhancing our understanding of the complex processes involved in tropical cyclones (Hristova-Veleva et al., 2020).



# Journal of Geophysical Research: Space Physics

10.1029/2024JA032933

The need for simultaneous measurements of neutral winds, temperatures, and electron density during hurricanes is increasingly recognized. Wind stress and heat flux in storm conditions, both influenced by neutral winds and temperatures, have important roles (Geernaert et al., 1987). Moreover, the intricate effects of storms on electron density and the ionosphere contribute to the importance of comprehensive measurements (Amayenc & Vasseur, 1972; Mendillo & Klobuchar, 2006). The significance of storm-induced changes in neutral composition, and their potential to improve hurricane prediction, have also been underscored (Zhu et al., 2002).

Satellite observations have also helped advance our understanding of hurricane-induced GWs. For instance, the proposed GHOST mission concept involves using a midinfrared imager on a geostationary satellite to monitor the Atlantic hurricane belt. This aims to utilize GW observations for predicting tropical cyclone rapid intensification and enhancing the characterization of upper-atmospheric GWs with high spatial and temporal resolution (Tratt et al., 2018).

Furthermore, ionospheric and satellite observations have proven effective in studying the dynamic behavior of hurricanes and detecting severe storms (Dewan et al., 1998; Hung, 1981; Hung & Smith, 1978). Satellite data have confirmed the influence of wind speed and forward movement on wave height in hurricanes (Hung & Smith, 1981; Young & Burchell, 1996). The first spaceborn GNSS-Reflectometry (GNSS-R) observations of hurricanes confirmed the detection of changes in ocean conditions and near-surface wind associated with hurricanes (Foti et al., 2017). On a larger scale, the global impact of tropical cyclone-associated GWs has been quantified using satellite observations (Wright, 2019).

Among recent technological advances, the COSMIC-2 satellite, used in this paper, has provided some insight into hurricanes. By assimilating GNSS radio occultation bending angles from COSMIC-2 into the Hurricane Weather Research and Forecasting model, a reduction in forecast errors for minimum central sea level pressure and an improvement in intensity forecasts were observed (Miller et al., 2023). Deep GNSS radio occultation signals from COSMIC-2 that were observed below the Earth's limb and collocated with severe tropical cyclones indicate sharp inversion layers in the planetary boundary layer and show potential for detecting tropical cyclones due to strong vertical refractivity gradients (Hordyniec et al., 2022).

Despite these advances in observational and modeling techniques, most studies emphasize the need for more dedicated efforts to better characterize the upper atmospheric effects of hurricanes and understand the physical coupling mechanisms involved. While previous research has suggested ionospheric effects of hurricanes, the upper atmospheric impacts and induced GW activity remain insufficiently characterized due to a lack of comprehensive global thermospheric observations, particularly of winds and temperatures. However, recent technological advancements in space-borne observations continue to provide new opportunities to study vertical coupling during hurricanes. Our study addresses this gap by combining data from multiple advanced satellite systems.

This paper aims to characterize the upper atmospheric variations during *Hurricane Grace* that took place in August 2021, employing a suite of satellite observations. Specifically, we will utilize the Constellation Observing System for Meteorology, Ionosphere, and Climate-2 (COSMIC-2), Global-scale Observations of the Limb and Disk (GOLD), and Ionospheric Connection Explorer (ICON) satellites' coincident measurements at low-latitudes to study the neutral temperature, horizontal winds and dynamics in the mesosphere and thermosphere, and ionospheric electron density. This is the first study to combine these satellites' data to study long-range vertical coupling during a hurricane event. Our findings are expected to contribute to the ongoing efforts to characterize hurricane-induced gravity waves and their impacts on the upper atmosphere, potentially improving our ability to predict and understand these powerful meteorological events.

The paper is structured as follows: Data and methods are described in Section 2, providing details of the satellite instruments and data sets used in the study as well as the methodologies for data analysis. Section 2.1 provides a detailed account of Hurricane Grace's development, trajectory, and intensity. Our choice of analysis period and space weather conditions are presented in Section 2.2. Sections 2.3–2.5 describe COSMIC-2, ICON, and GOLD satellites, respectively. Results are presented in Section 3. In Section 4 observational results are discussed in detail, exploring the implications of the findings and how they align with current understanding. Summary of key findings and conclusions of our research are given in Section 5, along with recommendations for future research.



21699402, 2024, 10, Downloaded from https://agupubs.onlinelibrary.wiley.com/doi/10.1029/2024JA032933 by George Mason University, Wiley Online Library on [21/10/2024].

Figure 1. The best track of hurricane grace. Data obtained from the National Hurricane Center (2023). Radii and wind swath data are also included. The color scale represents the hurricane's wind speed. A  $10^{\circ} \times 11^{\circ}$  rectangular red box highlights the area used for Figure 7.

#### 2. Data and Methods

To characterize the impact of Hurricane Grace on the upper atmosphere and ionosphere, we first describe its selection criteria and explain the background space weather conditions. This study leverages data from three spacecraft: ICON, GOLD, and COSMIC-2 satellites.

#### 2.1. Hurricane Grace

Hurricane Grace occurred from 13th to 21st August 2021. It began as a tropical wave emerging from the west coast of Africa on August 9th, then developed and traveled south of the Cabo Verde Islands by August 10th. The system continued its westward track across the eastern Atlantic, propelled by a pace of about  $10.3 \text{ m s}^{-1}$ . An extended area of relatively low atmospheric pressure 1,200 nautical miles east of the Lesser Antilles was developed on August 12. Despite scatterometer data revealing wind speeds of 25–30 knots, a well-defined, closed surface circulation was not yet established (Beven, 2021; Brad et al., 2022). One knot is approximately  $0.51 \text{ m s}^{-1}$ .

On 13 August 2021, the data revealed a well-defined low-level circulation, which indicates the formation of a tropical depression (Brad et al., 2022). Figure 1 shows the best track of Hurricane Grace from 13 to 21 August. The system moved rapidly westward due to a large area of high atmospheric pressure in the subtropics. It had strengthened enough to become classified as a tropical storm by 14 August 2021. Grace's path had significant fluctuations in structure and intensity, and regained tropical storm status as it neared the Hispaniola island east of Cuba by August 16th. Critical factors like sea-surface temperatures and deep-layer wind shear were instrumental in its rapid intensification phase over the southwestern Gulf of Mexico. By 21 August Grace had intensified into a major hurricane, achieving a peak intensity as it made landfall along the coast of the Mexican state of Veracruz (Brad et al., 2022).

The rapid intensification can be seen during the 20 August in Figure 1. The environment of low to moderate deep-layer shear over 30°C sea-surface temperatures was conducive to this intensification. Overall, the hurricane's center was constrained within 7 degrees of latitude, and travels longitudinally from –45° to its landfall near –98°. Figure 2 presents satellite imagery of Hurricane Grace. The imagery is taken from the Geostationary Operational Environmental Satellites (GOES), a collaborative NOAA and NASA program providing continuous imagery and data on atmospheric conditions and space weather. These images utilize a "sandwich" product technique designed for monitoring deep convective activities within storm systems. This method merges high-resolution visible imagery with color-enhanced infrared (IR) window images, offering a composite view of the morphological characteristics and thermal properties of cloud tops. Complementing the satellite imagery, Figure 2 also shows plots derived from the MERRA-2 data set product M2I3NPASM. We plot wind speed and vector data at an altitude of 5 km, aligning with the timing and geographical extent of the satellite observations of Hurricane Grace, specifically centered around the rapid intensification on 20 August.

21699402, 2024, 10, Downl

from https://agupubs.onlinelibrary.wiley.com/doi/10.1029/2024JA032933 by George Mason University, Wiley Online Library on [21/10/2024]. See

**Figure 2.** NOAA satellite imagery of the hurricane with selected dates from August 17th to August 22nd. Underneath each satellite image is a MERRA-2 wind speed and vector plot at 5 km. Scale vector arrows of 10 ms<sup>-1</sup> are provided. The colorbar represents different wind speeds.

#### 2.2. Choice of Analysis Period and Space Weather Conditions

The analysis of Hurricane Grace's impact on the thermosphere necessitated a period characterized by minimal solar and geomagnetic disturbances. This prerequisite stems from the thermosphere's sensitivity to variations in solar and geomagnetic activity, which can significantly impact its temperature, density, and wind patterns, especially during magnetic storms (Yiğit, Frey, et al., 2016). Figure 3 shows the space weather conditions during Hurricane Grace. Panel (a) shows the magnetic activity through the  $A_p$  index, and panel (b) depicts the solar activity gauged by the  $F_{10.7}$  solar radio flux. The gray shading across both panels marks the primary focus period of the study. Both 2020 and 2021 are plotted. 2020 did not have a hurricane during the period Grace occurred in 2021, and is used for comparison throughout the rest of this paper. We aim to mitigate the confounding influence of external space weather variables.

Grace's trajectory, which is characterized by its consistent latitudinal position, extensive longitudinal path, and rapid intensification on 20 August, provided an ideal candidate for our study. Additionally, the hurricane's path and timing benefited from optimal satellite coverage.

#### 2.3. **COSMIC-2**

The COSMIC-2 satellite, a joint initiative between the American Institute in Taiwan (AIT) and the Taipei Economic and Cultural Representative Office in the United States (TECRO), provides unprecedented spatial-temporal sampling of the middle- to low-latitude ionosphere. It was launched on 25 June 2019, and comprises six satellites which were maneuvered to their operational orbits at around 550 km altitude. The primary instruments, the Tri-GNSS Radio-occultation System (TGRS), the Ion Velocity Meter (IVM), and a Radio Frequency Beacon (RFB), work in tandem to produce many space weather products including relative total electron content (TEC), scintillation amplitude index (S4), and electron density profiles (Anthes & Schreiner, 2019; Fong et al., 2019; Yue et al., 2014).

Analyses often involve vertical integration of electron density profiles up to 550 km to obtain ionospheric TEC (ITEC), followed by detailed statistical and tidal analysis to discern patterns in ionospheric variability (Lin et al., 2012; N. Pedatella, 2022). The precision and reliability of the COSMIC-2 data have been demonstrated through comprehensive validation efforts. Early comparisons of relative TEC observations and electron density

21699402, 2024, 10, Downloaded from https://agupubs.onlinelibrary.wiley.com/doi/10.1029/2024JA032933 by George Mason University. Wiley Online Library on [21/10/2024]. See the Term

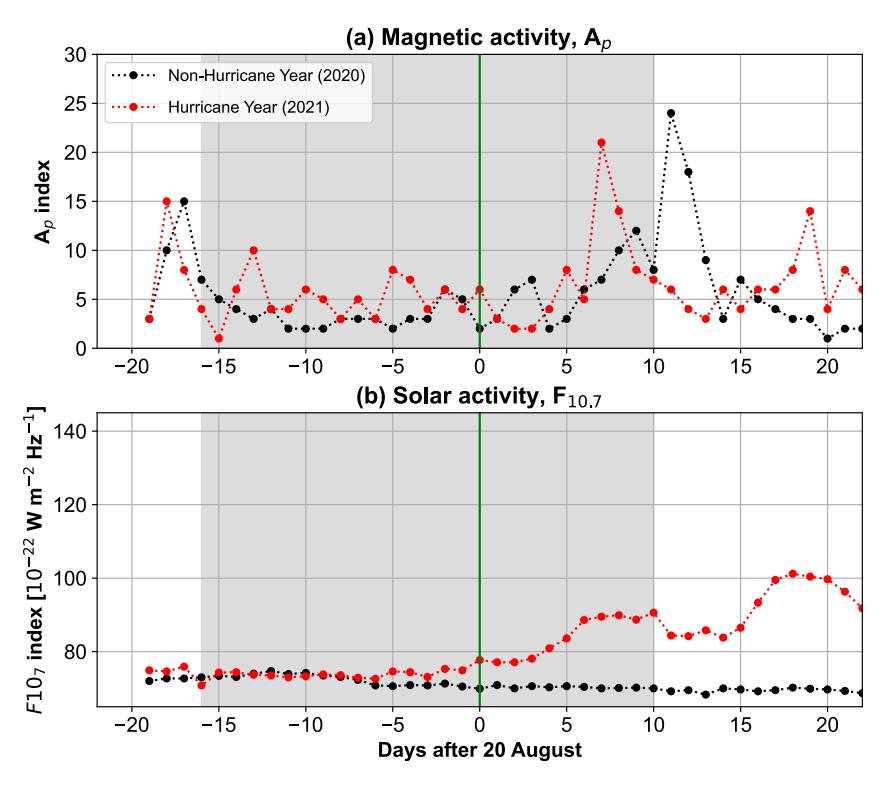


Figure 3. Space weather conditions during Hurricane Grace. Panel (a) shows the magnetic activity in terms of the  $A_p$  index. Panel (b) shows the solar activity measured by the  $F_{10.7}$  solar radio flux. Gray shadings represent the main time period focused on for this study. Red dotted lines represent the conditions during August and September 2021 while the black dotted lines are the data from 2020, a non-hurricane year.

profiles with ground-based measurements have confirmed the high accuracy and consistency of the satellite data (N. M. Pedatella et al., 2023).

Unlike previous satellites, COSMIC-2's dense sampling allows investigation into the short term variability into the ionosphere during hurricanes. The high-resolution continuous data facilitates the observations of short-term variations in electron density. This study leverages the COSMIC-2's capabilities to examine diurnal and zonal mean electron density during the 2021 Hurricane Grace, revealing longitudinal characteristics in greater detail (J.-Y. Liu et al., 2022).

During Hurricane Grace we observed sufficient data coverage. Figure 4 illustrates the spatiotemporal coverage of COSMIC-2 of the retained profiles. Panels (a), (b), and (e) show longitude, latitude, and local time coverage as a function of UTC, respectively. Panels (c), (d), and (h) show the altitude, latitude, and longitude as a function of local time, while panel (f) shows the altitude versus latitude distribution and panel (g) shows the latitude versus longitude distribution. Scatter-points are color coded corresponding to the date of observation in 2021.

#### **2.4. ICON**

The Ionospheric Connection Explorer (ICON) observed the low- to middle-latitude thermosphere between  $10^{\circ}$  S and  $40^{\circ}$ N (Immel et al., 2018a, 2018b). Launched on 10 October 2019 and operated till 25 November 2022, ICON observed the low-latitude thermosphere-ionosphere system above 90 km in unprecedented detail, aiming to aid the understanding of complex interactions between Earth's upper atmosphere and the broader geospace environment.

For this study, we utilize ICON's Michelson Interferometer for Global High-resolution Thermospheric Imaging (MIGHTI) instrument data, focusing on the period during Hurricane Grace. MIGHTI provided observations of the zonal (u) and meridional (v) wind components by measuring the Doppler shifts of atomic oxygen's green line ( $\lambda = 557.7$  nm) and red line ( $\lambda = 630$  nm) emissions, providing a detailed view of thermospheric circulation and

21699402, 2024, 10, Downloaded from https://agupubs.onlinelibrary.wiley.com/doi/10.1029/2024JA032933 by George Mason University, Wiley Online Library on [21/10/2024]. See the Terms

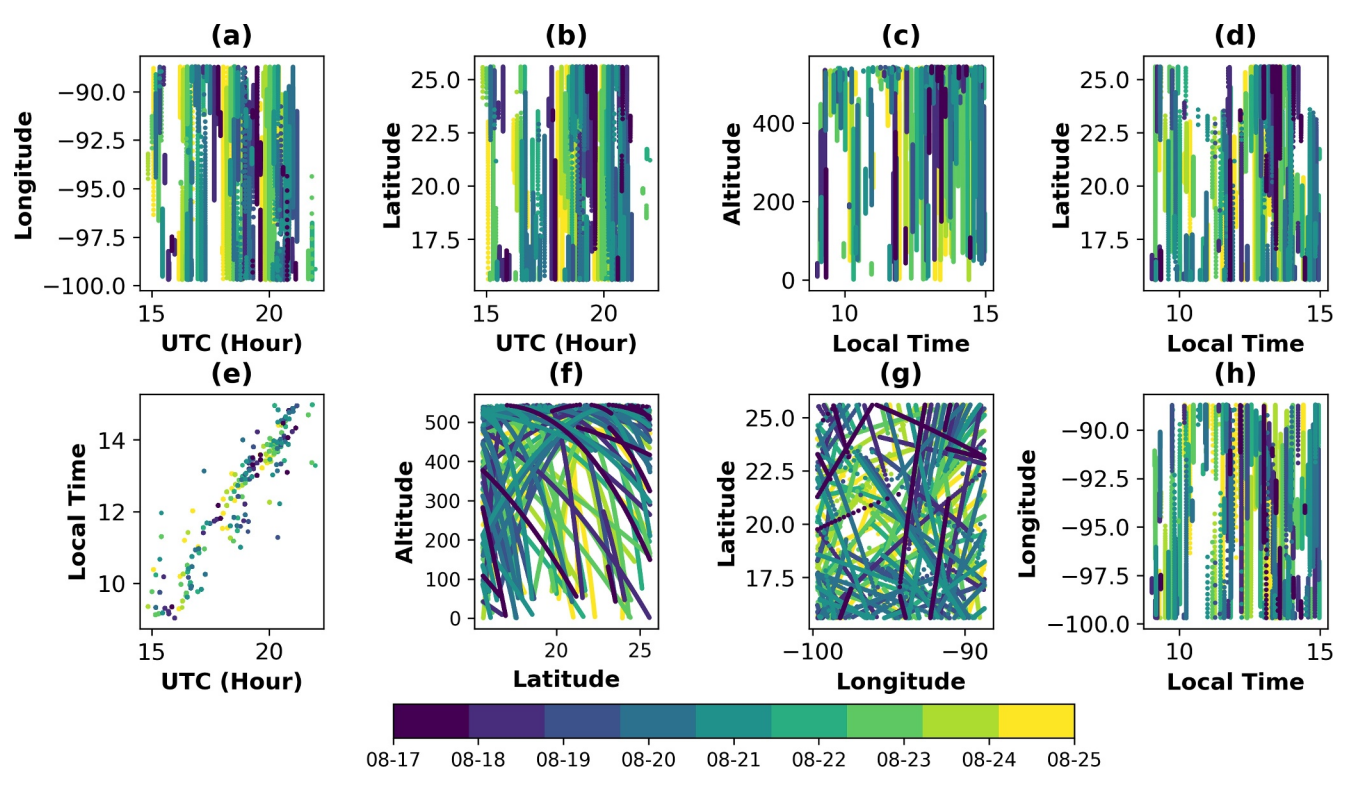


**Figure 4.** Spatiotemporal coverage of COSMIC-2 observations during Hurricane Grace. Panels (a), (b), and (e) show the longitude, latitude, and local time as a function of UTC, respectively. Panels (c), (d), and (h) show the altitude, latitude, and longitude as a function of local time, respectively. Panel (f) shows the altitude-latitude distribution while panel (g) shows the latitude-longitude distribution. Colored markers indicate the date of the retained observations. All dates are from 2021.

wind variations (Englert et al., 2017). The data set comprises version 5 zonal and meridional winds derived from both green and red line measurements. MIGHTI's green line observations span altitudes from approximately 90 to ~200 km during daytime and narrow to 90 to ~115 km for both day and night coverage. Red line data cover around 150–300 km altitude. The vertical sampling is 3 and 10 km altitude bins for the green and red line data, respectively. Daytime wind measurements are conducted at about 30 second cadence, while nighttime observations occur every ~60 seconds. By pairing line-of-sight (LOS) wind measurements from MIGHTI's dual sensors we acquire detailed northward and eastward wind component data. The quality of these observations is assessed, with each measurement assigned a quality flag to ensure reliability in further analyses (Harding et al., 2021). ICON/MIGHTI winds have been extensively used to study vertical coupling during quiet and transient periods, in particular, to study semidiurnal-induced vertical coupling (Forbes et al., 2022), global-scale waves (Gasperini et al., 2023), connection between plasma drifts and neutral winds (Zhang et al., 2022) and the response of the thermospheric circulation during a major SSW (Yiğit et al., 2024).

During the August 2020 and August 2021 analysis periods, we observed sufficient data coverage across the targeted longitudes and latitudes that coincided with the hurricane. Figure 5 shows the latitude versus local time evolution of ICON measurements during August in 2020–2022. There were no hurricanes in August 2022, but we decided to exclude 2022 from our analysis because of the insufficient latitudinal coverage during the same local times compared to the previous years. Our focus on ICON/MIGHTI version 5 zonal and meridional winds from both green and red line measurements during the Hurricane Grace period aims to explain the spatiotemporal variability in instantaneous horizontal winds. Previous ICON observations provided indirect evidence of momentum deposition by small-scale gravity waves, contributing to our understanding of the thermosphere's dynamics during such meteorological phenomena (Yiğit et al., 2022). The inclusion of a complementary analysis for August 2020, without a hurricane event, offers a better view of the hurricane-induced variations in mean winds and thermospheric circulation. Through careful data selection and quality control, excluding outliers and bad flagged data, we ensure the integrity and statistical significance of these findings. Utilizing multiple days of continuous ICON observations allows for a comprehensive analysis of longitudinally averaged winds and

21699402, 2024, 10, Downloa

from https://agupubs.onlinelibrary.wiley.com/doi/10.1029/2024JA032933 by George Mason University, Wiley Online Library on [2]/10/2024]. See the Terms

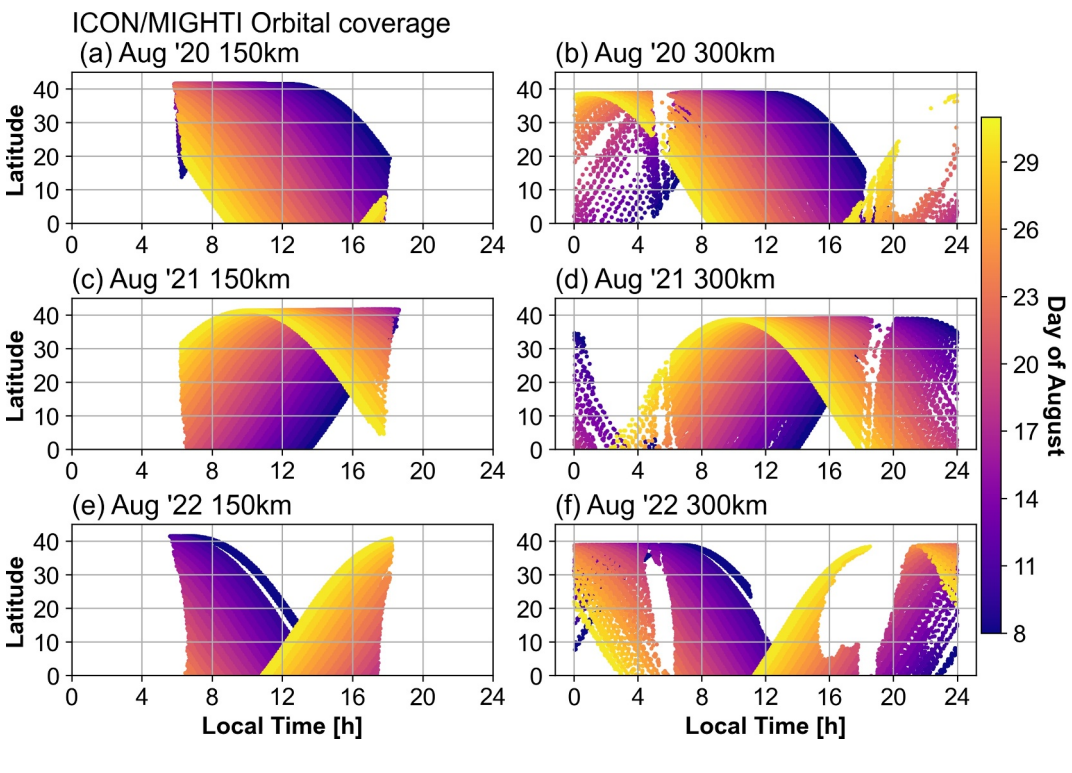


**Figure 5.** Altitude versus local time of retained ICON orbits. Three months are plotted: August 2020, August 2021, and August 2022. The different colors represents different days of the month. Panels (a), (c), and (e) are from 150 km altitudes, while (b), (d), and (f) show the coverage at 300 km.

circulation patterns. In the results to be presented, the data are binned with respect to altitude, longitude, local time, and solar zenith angle, which reveals intricate dynamics of the thermosphere, showcasing the day-to-day variability of the zonal and meridional winds during the hurricane.

#### 2.5. GOLD

The Global-scale Observations of the Limb and Disk (GOLD) (Eastes et al., 2017) satellite operates from a geostationary orbit, capturing the Far Ultraviolet (FUV) spectrum of Earth's atmosphere from 0610 to 0040 Universal Time (UT) every day. Thermospheric temperatures are derived from the  $N_2$  Lyman-Birge-Hopfield (LBH) emission profile at a height of approximately 150 km. This procedure also accounts for a constant background term, a wavelength shift, and a scale factor to align the forward model's LBH spectrum brightness with observed values (Eastes et al., 2020a, 2020b). We utilize version 5 of the level 2 "Tdisk" data product, carefully filtering out data flagged as unusable by the dqi flags at both file and pixel levels to ensure data reliability. To increase the signal-to-noise ratio and focus on daytime observations, the observations of solar zenith angles ( $\chi$ ) greater than 80 have been removed. "Daytime" in the context of GOLD data does not correspond to specific local time ranges, but rather to periods when the observed area is sunlit according to the solar zenith angle criterion.

During this period, while the geomagnetic and solar activity was predominately low, it briefly peaked to an Ap index of 21 following the hurricane. This study excludes data from days with an Ap index greater than 15 to mitigate the influence of heightened geomagnetic activity on thermospheric temperatures. The data files are systematically processed to extract and filter the necessary observations. Temperatures outside the range of 300–1300 K are discarded to remove anomalies. The filtering also involved weighted observations based on their relative uncertainty to prioritize more reliable measurements, emphasizing data points with lower relative uncertainty.

Figure 6 presents GOLD data spatiotemporal coverage from a representative day, 18 August 2021. Only the filtered measurements are presented. Panels (a)–(c) show the longitude, latitude, and solar zenith angle evolution

21699402, 2024, 10, Downloaded

from https://agupubs.onlinelibrary.wiley.com/doi/10.1029/2024JA032933 by George Mason University, Wiley Online Library on [21/10/2024]. See the Terms and Conditions

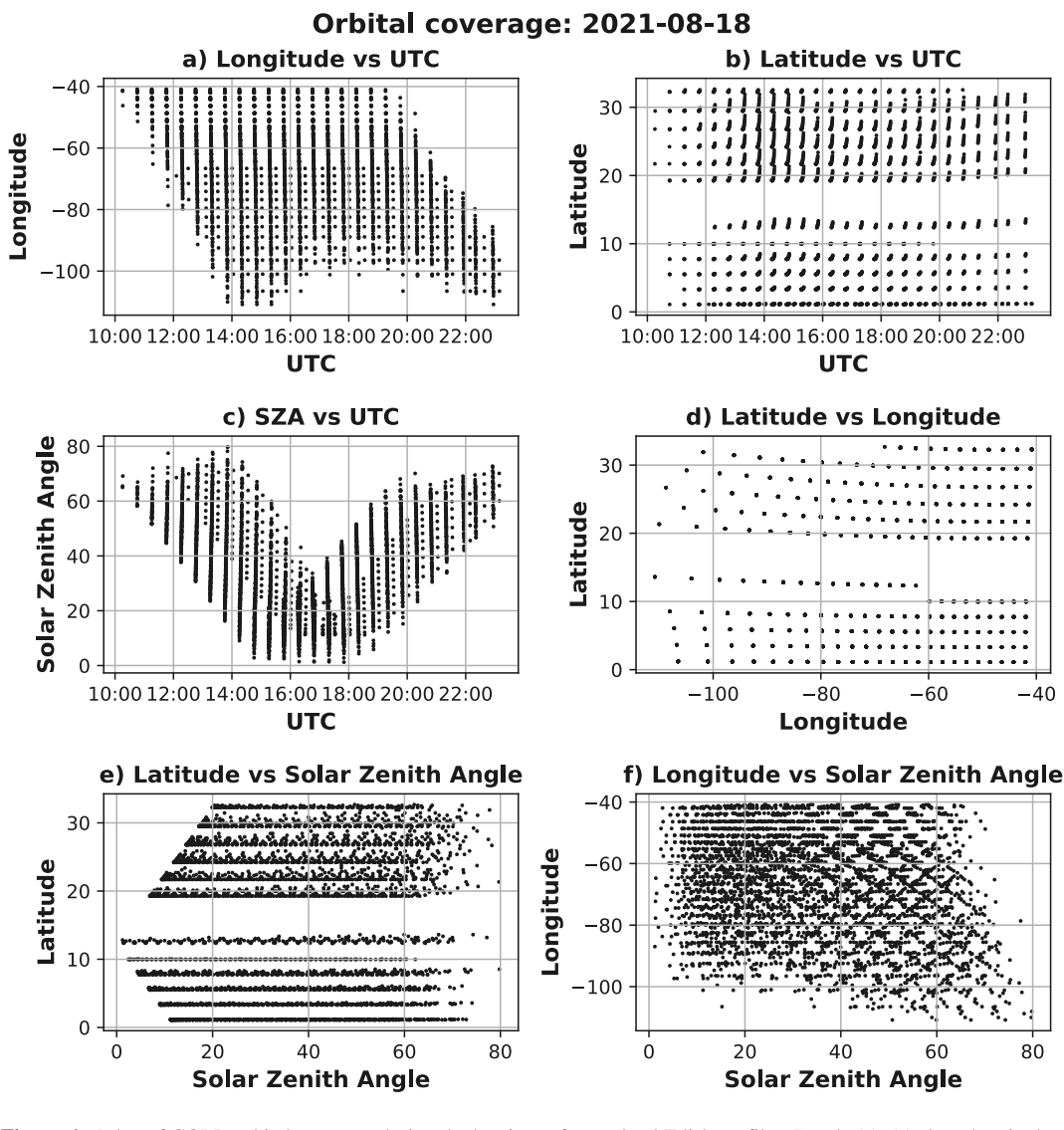


**Figure 6.** 1 day of GOLD orbital coverage during the hurricane for retained Tdisk profiles. Panels (a)–(c) show longitude, latitude, and solar zenith angle as a function of UTC, respectively. Panel (d) shows the latitude-longitude distribution. Panels (e) and (f) show the latitude and longitude as a function of solar zenith angle, respectively.

with UTC, respectively. Panel (d) shows the latitude versus longitude of the measurements. There is a small data gap in between latitudes 10°N and 20°N. The GOLD data extends to slightly above 30°N, which is smaller than the usual extent of 70°N. Panels (e) and (f) shows the latitude and longitude as a function of solar zenith angle, respectively. The small gap in coverage between latitudes 10°N and 20°N is seen here as well. There is good longitudinal coverage over the area of Hurricane Grace although some of the higher solar zenith angle measurements ( $\chi > 70^\circ$ ) were removed during the filtering process.

#### 2.6. Data Analysis Methods

The analysis starts with the preprocessing of the satellite data, followed by the extraction of relevant parameters for this study, such as electron density  $(n_e)$ , horizontal wind speeds (u,v), and temperatures (T). The data is then time-aligned and geolocated to match the temporal and spatial progression of Hurricane Grace. Statistical analysis methods are used to identify significant changes and anomalies in the parameters associated with the hurricane. The data from different satellites are compared and cross-validated to ensure consistency and reliability of the results. The potential influence of other geophysical and space weather phenomena is also accounted for in the



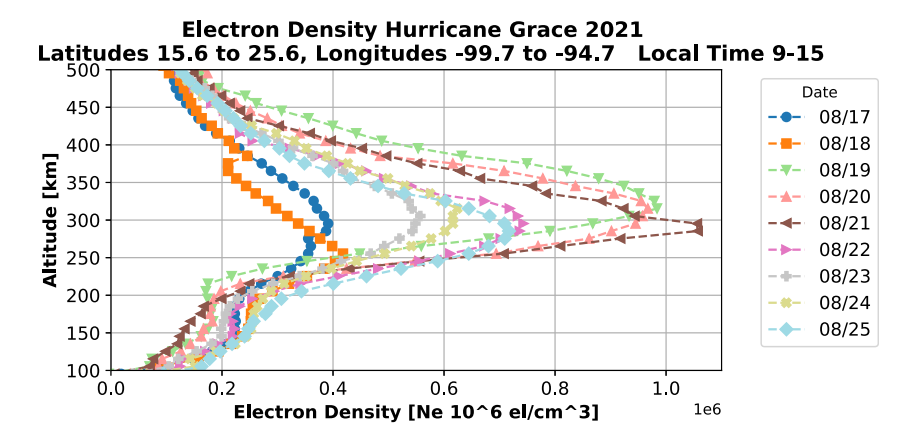


**Figure 7.** Variation of electron density with altitude in the ionosphere above Hurricane Grace's rapid intensification zone, observed from COSMIC-2. Each line represents a different data between August 14th and 25 August 2021, capturing local times from 9 to 15 hr. The altitude range is  $100-500 \, \text{km}$  across latitudes  $15.6^{\circ}$  to  $25.6^{\circ}$  and longitudes  $-99.7^{\circ}$  to  $-94.7^{\circ}$ . This range is highlighted in Figure 1. A marked increase in electron density is noted on August 19th, 20th, and 21st, coinciding with the hurricane's peak intensity. The following Table 1 depicts  $N_m E_2$  and  $h_m E_2$  for each day. The altitudes are binned in 5 km bins.

analysis. In the next steps, the observed changes are analyzed in the context of the evolution of the hurricane. The temporal correlation between the intensification of the hurricane and the observed changes in the upper atmosphere is assessed. Potential causal mechanisms for the observed changes are explored, leveraging the existing literature on atmospheric dynamics and vertical coupling processes.

#### 3. Results

#### 3.1. Ionospheric Electron Density Variations

In Figure 7, we present the day-to-day variations in electron density profiles within the ionosphere directly above the region experiencing the rapid intensification and subsequent landfall of Hurricane Grace. The analysis spans latitudes from  $15.6^{\circ}$ N to  $25.6^{\circ}$ N and longitudes from  $-88.7^{\circ}$  to  $-99.7^{\circ}$ , that is, a  $10^{\circ} \times 11^{\circ}$  latitude × longitude region. This region is highlighted with a red box in Figure 1. Each line represents the mean profile for 1 day through August 17th–25th 2021, derived from multiple COSMIC-2 measurements within the local time range of 9–15 hr. This time range captures a considerable portion of the daytime ionosphere, including periods of typically high ionization. The average local time for each day's measurements is included in Table 1.  $N_m F_2$  and  $h_m F_2$  naturally vary throughout the day; the averaging over a 6-hr period may smooth out some of this variability, but it allows the observation of general trends across multiple days (Venkatesh et al., 2011). There are substantial increases in electron density from approximately  $0.6 \times 10^6$  to nearly  $9.8 \times 10^5$  cm<sup>-3</sup> on August 19th, 20th, and 21st. These increases correspond to the days of Hurricane Grace's peak intensity and are particularly pronounced

**Table 1** Data of  $N_m F_2$ ,  $H_m F_2$ , and Average LT Over Several Days

Date	$N_m F_2$ [el/cm <sup>3</sup> ]	$H_m F_2$ [km]	Average LT [h]
08-17-21	$3.912 \times 10^5$	295.4	12.45
08-18-21	$4.179 \times 10^5$	255.4	11.65
08-19-21	$9.837 \times 10^5$	315.4	13.63
08-20-21	$9.671 \times 10^5$	315.4	12.72
08-21-21	$1.057 \times 10^6$	285.4	12.98
08-22-21	$7.432 \times 10^5$	295.4	12.56
08-23-21	$5.573 \times 10^5$	305.4	12.55
08-24-21	$6.238 \times 10^5$	315.4	12.81
08-25-21	$7.170 \times 10^5$	285.4	12.66

in the F-region ionosphere. A change in  $h_m F_2$  is observed between August 18 and 19, with values shifting from 255 to 315 km, respectively. This 60 km increase coincides with a difference in the average measurement times, with data from August 18th having an earlier average local time of 11.65 hr compared to 13.64 hr for August 19. The phase of the diurnal component of  $h_m F_2$  varies slightly between 1130 and 1300 LT, indicating a rise in  $h_m F_2$  during this period (Zolotukhina et al., 2014). Both  $f_o F_2$  and  $h_m F_2$  contain quasi-harmonic oscillations with diurnal and semidiurnal components being the strongest (Zolotukhina et al., 2011). These diurnal variations are likely due to solar heating, changes in neutral composition, and electrodynamic effects. However, the magnitude of this change is substantial for around a 2-hr time difference, suggesting that additional factors could be contributing. The data suggest a dynamic response in the ionosphere coincident with the hurricane, indicating long-range vertical coupling mechanisms during these conditions.



21699402, 2024. 10, Downloaded from https://agupubs.onlinelibrary.wiley.com/doi/10.1029/2024JA032933 by Gorge Mason University, Wiley Online Library on [21/10/2024]. See the Terms and Conditions (https://onlinelibrary.wiley.com/doi/10.1029/2024JA032933 by Gorge Mason University, Wiley Online Library on [21/10/2024]. See the Terms and Conditions (https://onlinelibrary.wiley.com/doi/10.1029/2024JA032933 by Gorge Mason University, Wiley Online Library on [21/10/2024]. See the Terms and Conditions (https://onlinelibrary.wiley.com/doi/10.1029/2024JA032933 by Gorge Mason University, Wiley Online Library on [21/10/2024]. See the Terms and Conditions (https://onlinelibrary.wiley.com/doi/10.1029/2024JA032933 by Gorge Mason University.

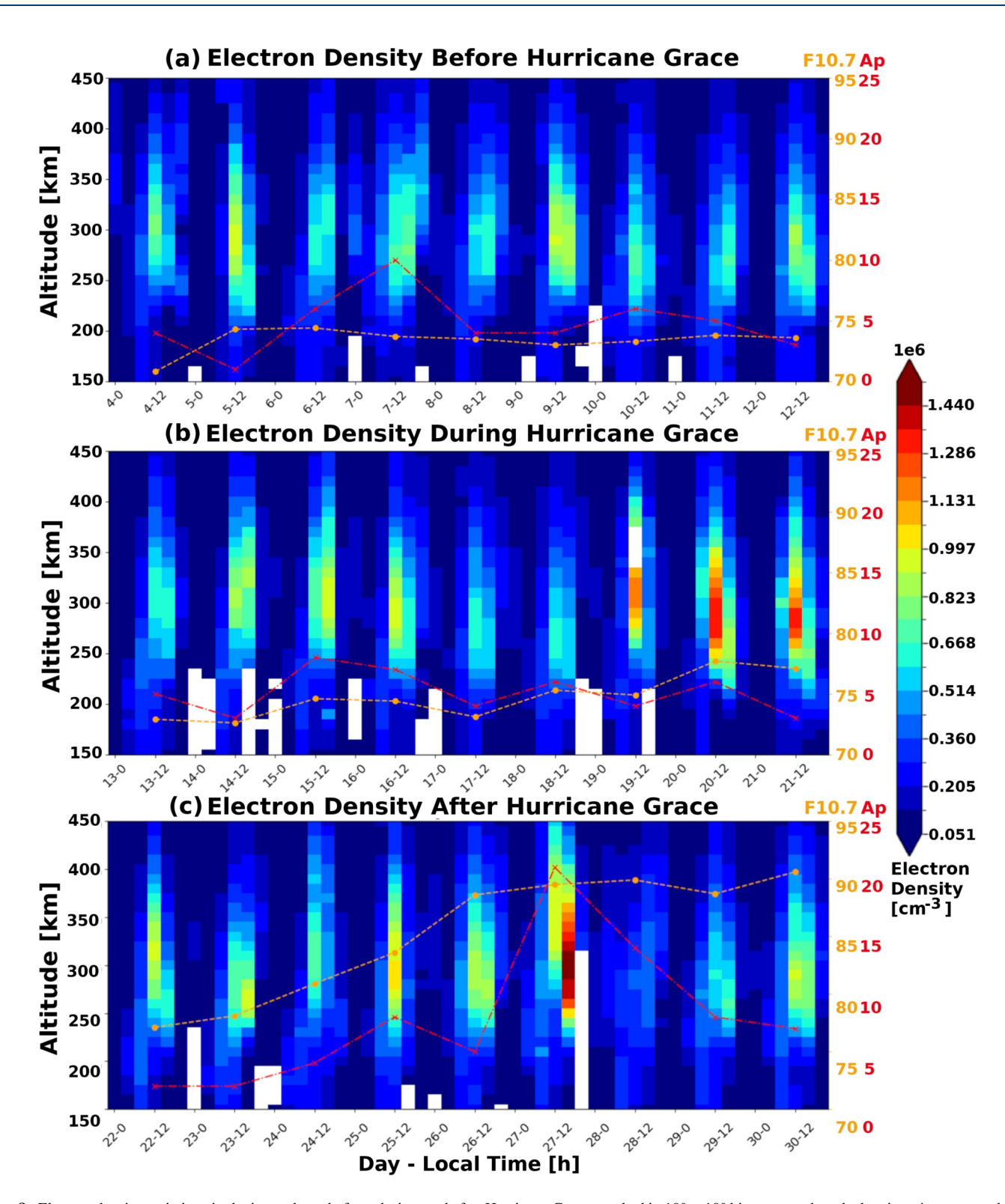


Figure 8. Electron density variations in the ionosphere, before, during, and after Hurricane Grace, tracked in  $10^{\circ} \times 10^{\circ}$  bins centered on the hurricane's center each day. Panel (a) illustrates conditions 9 days prior, panel (b) shows during the hurricane, while panel (c) shows the 9 days following the event. The altitude ranges from 150 to 450 km, and local time is segmented into 4-hr bins along the *x*-axis. The *x* axis is sorted into day and local time bins, with the convention (day number in august—local time). The color scale indicates electron density (in  $elcm^{-3}$ ), with overlaid F10.7 solar flux (orange) and geomagnetic Ap index (red). White shading represents missing or filtered data.

21699402, 2024, 10, Downloaded from https://agupubs.onlinelibrary.wiley.com/doi/10.1029/2024JA032933 by George Mason University, Wiley Online Library on [21/10/2024]. See the Terms and

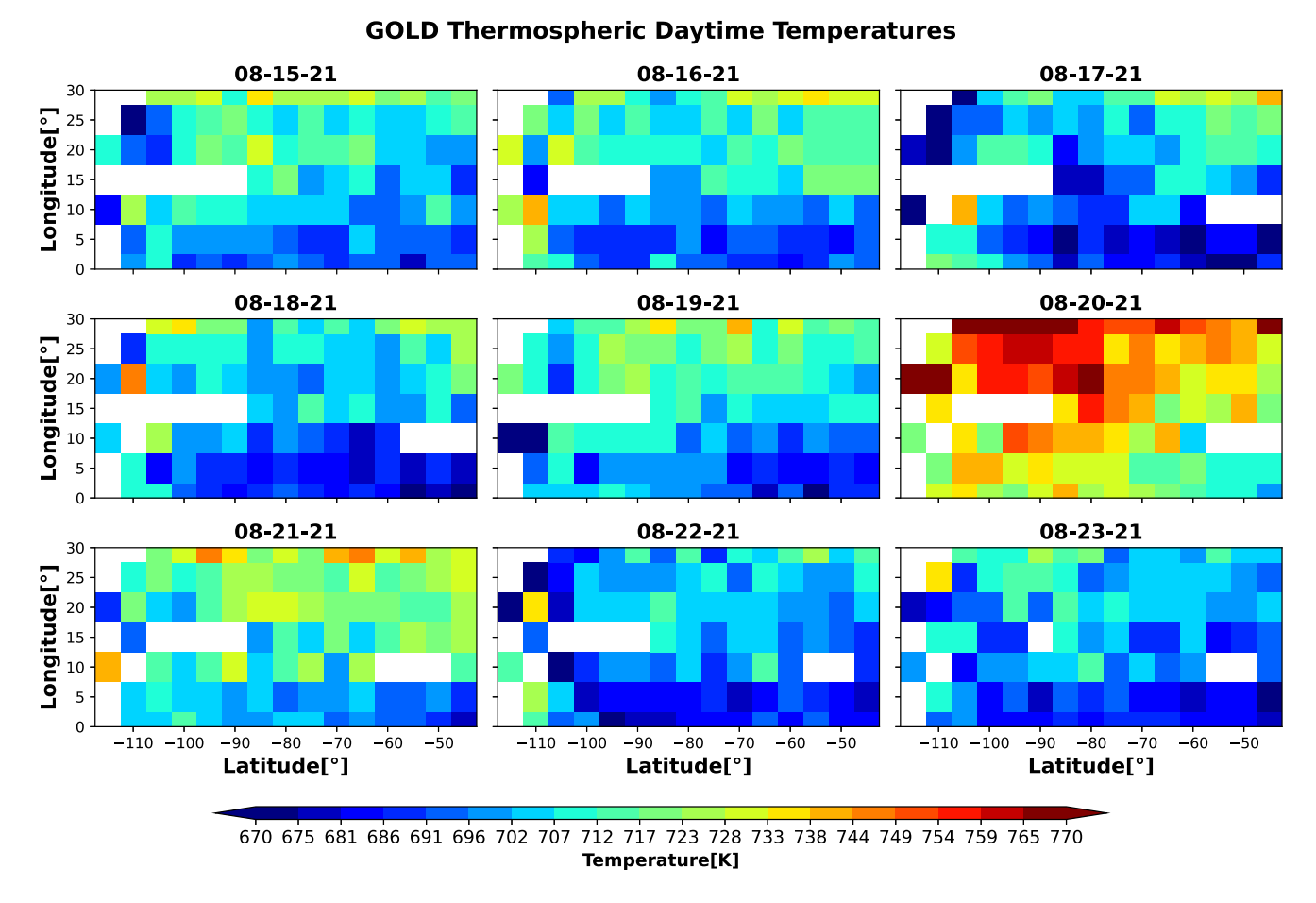


Figure 9. Daytime thermospheric temperatures around 150 km from GOLD are presented as longitude-latitude distributions. The data are organized in 5° latitude-longitude bins.

Figure 8 displays the electron density distributions in the E- and F-region ionosphere from 150 to 450 km during three distinct phases relative to Hurricane Grace to show electron density variation before, during and after the hurricane. The progression follows the hurricane's path, with latitudinal and longitudinal bins adjusted to remain centered on the storm, thus allowing for a consistent comparison of electron densities at equivalent local times. Time is presented on the x-axis, categorized by both the day and local time in 4-hr bins, highlighting diurnal variations. We observe pronounced increases in electron density between 200 and 380 km. On the 19th, 20th, and 21st, the electron density surge is marked with a peak on the 20th August showing a rise from about  $0.55 \times 10^6$  to  $1.3 \times 10^6$  cm<sup>-3</sup> at approximately 300 km altitude. The third panel shows the hurricane aftermath. A spike in electron density is noted on the 27th; however, its correlation with an Ap index exceeding 20 suggests the influence of a geomagnetic storm rather than lingering effects from Hurricane Grace.

#### 3.2. Thermospheric Temperatures

To assess hurricane-induced thermal changes in the thermosphere, we next consider observations from GOLD of thermospheric temperatures. Figure 9 displays the daytime thermospheric temperatures around 150 km altitude, as measured by GOLD. Covering the period from 15th to 23rd August 2021, temperatures are presented in 5° latitude and longitude bins across a region ranging from 0° to 30°N latitude and  $-115^{\circ}$  and  $-45^{\circ}$  longitude. The data highlight substantial warming during the rapid intensification of Hurricane Grace, specifically around August 19, 20, and 21. The greatest warming is on August 20th, which aligns closely with the peak electron density enhancements observed in the ionosphere during the storm.

Figure 10 shows the daytime thermospheric temperature differences using 17 August 2021, which is a few days before the hurricane's rapid intensification, as the baseline reference day. Subsequent days have this reference

21699402, 2024, 10, Downloaded from https://agupubs.onlinelibrary.wiley.com/doi/10.1029/2024JA032933 by George Mason University, Wiley Online Library on [21/102024]. See the Terms and Conditions (https://onlinelibrary.

## **Temperature Differences Relative to 08-17**

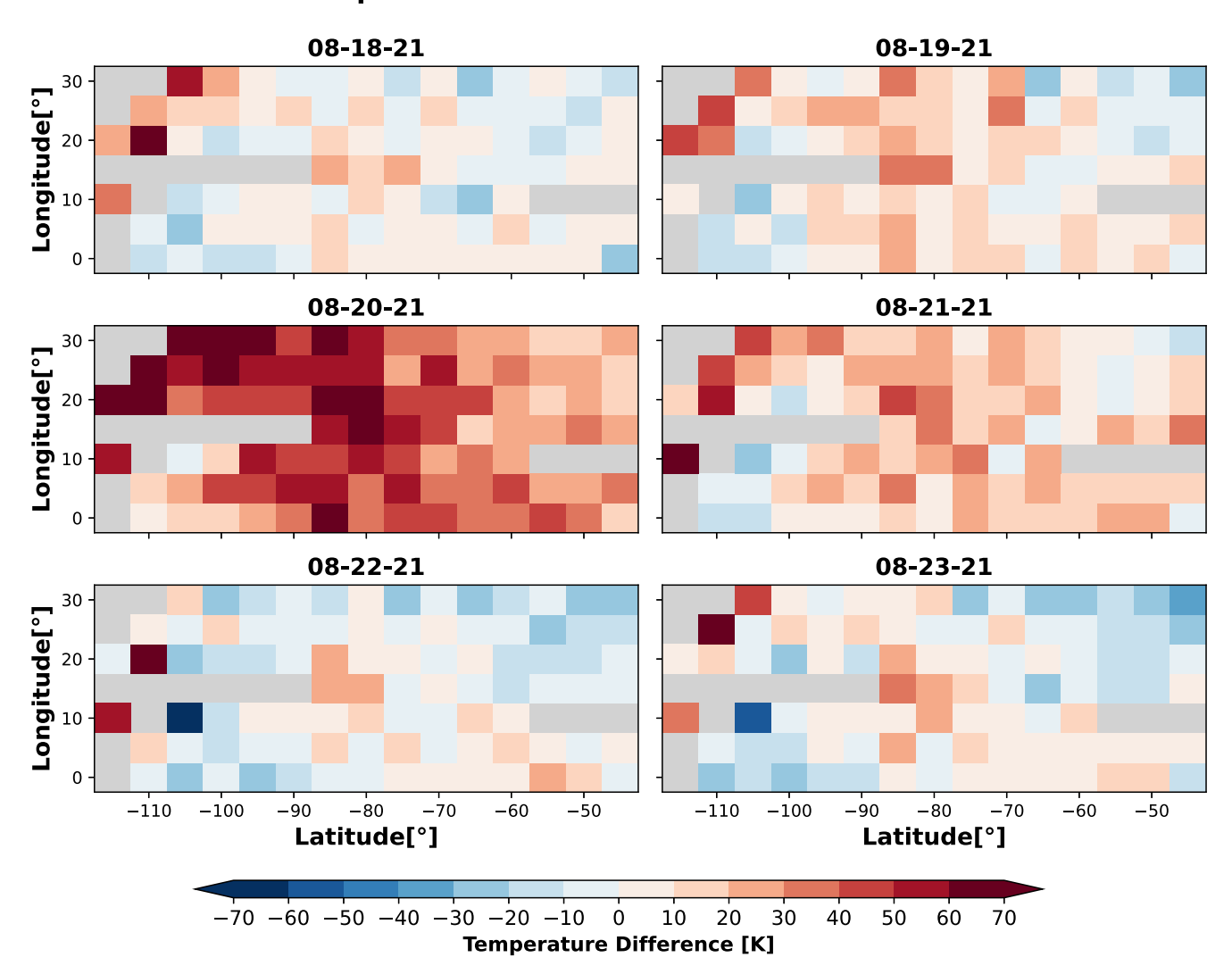


Figure 10. Daytime thermospheric temperature difference. 17 August 2021 is taken as a reference day and subtracted from the subsequent days. Red colors indicate a temperature increase.

subtracted from them to illustrate temperature changes induced by the hurricane. Areas depicted in red indicate an increase in temperature. Regions of pronounced warming are clearly visible around August 20th, directly correlating with the most intense phase of Hurricane Grace. This provides further evidence for the thermodynamical impact of the hurricane on the thermosphere.

Figure 11 shows the daytime thermospheric temperatures as a function of both latitude/longitude and solar zenith angle ( $\chi$ ), with  $\chi$  binned and excluding angles greater than 80° to avoid low-quality measurements and solar terminator effects. A different perspective of the significant warming on August 20th at around 25°N latitude and -95° longitude, near the hurricane's center, is seen. The temperature increase spans low-latitudes latitudes (10° to 35°N), with a positive gradient as latitude increases. This gradient is also evident in longitudes between -60° and -110°, where the maximum observed temperatures reach around 750 K. A less significant warming is noticed on August 25th, likely stemming from geomagnetic disturbances instead of hurricane caused disturbances.

21699402, 2024, 10, Downloaded from https://agupubs.onlinelibrary.wiley.com/doi/10.1029/2024JA032933 by George Mason University, Wiley Online Library on [21/10/2024]. See the Terms

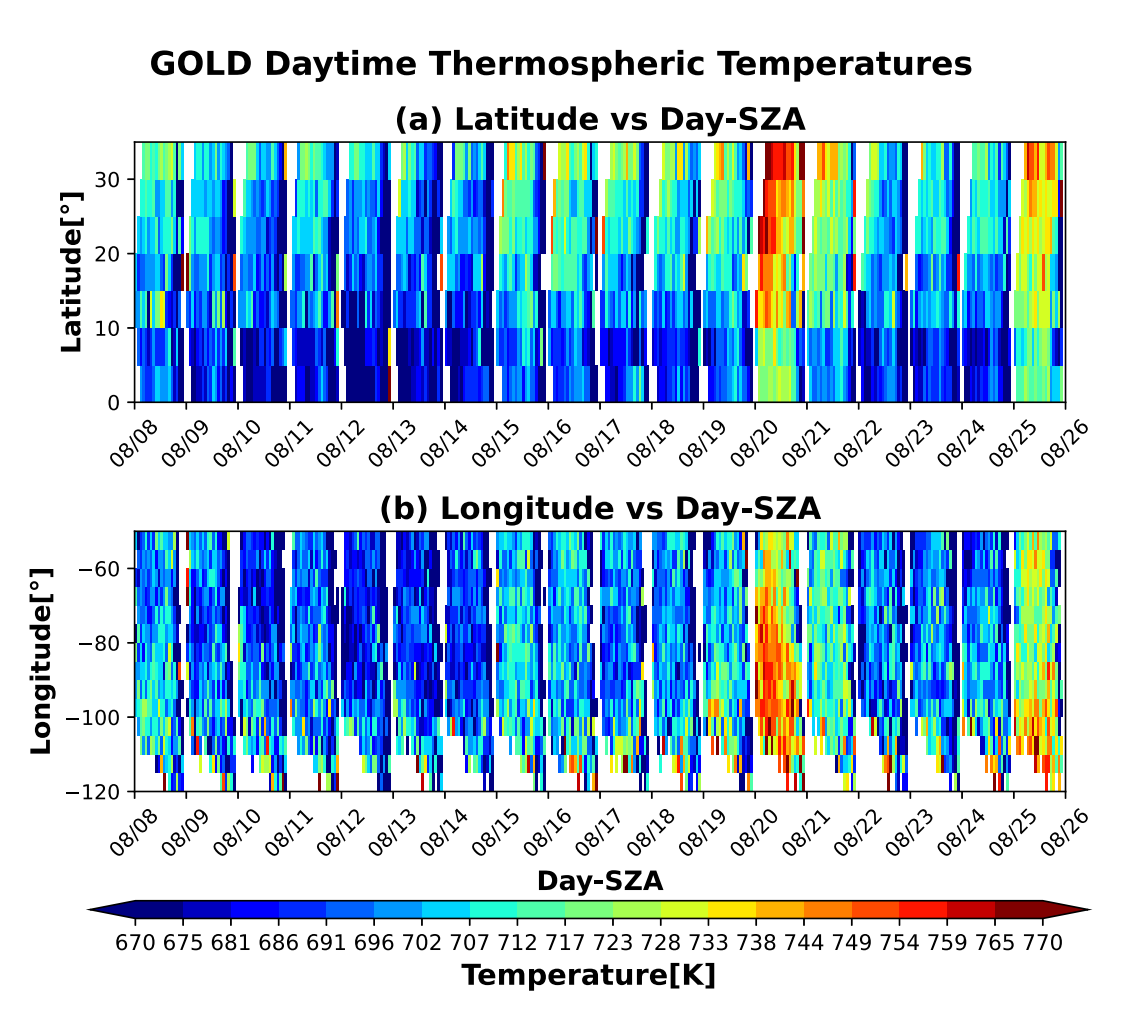


Figure 11. Daytime thermospheric temperatures. Panel (a) is plotted as a function of latitude while panel (b) is a function of longitude. The x axis is binned by day and solar zenith angle. Solar zenith angles greater than 80 have been excluded. The latitude and longitude are averaged in  $5^{\circ}$  bins.

#### 3.3. Thermospheric Circulation

The changes in thermospheric temperature and electron density during Hurricane Grace's intensification suggest dynamic atmospheric interactions. We next study the response of thermospheric circulation to the passage of the hurricane. Figure 12 shows an altitude versus day plot of the mean zonal (u) and meridional (v) winds from 90 to 300 km between the non-hurricane year (August 2020, left) and the hurricane year (August 2021, right), using data from the ICON/MIGHTI instrument. This data represents a fixed location from latitudes  $10^{\circ}$  to  $30^{\circ}$ N, longitudes  $-105^{\circ}$  to  $-75^{\circ}$ , and local time coverage from 7 to 17 hr. The black dashed lines across the panels represent the day of Hurricane Grace's rapid intensification, August 20th, providing a reference point to evaluate horizontal wind changes. For the zonal winds in the higher altitude range of 190-300 km, panels (a) and (b) reveal a westward (more negative) enhancement during the non-hurricane year. During 2021 the onset of the westward enhancement appears less pronounced and disrupted by the hurricane's intensification, suggesting a long-range coupling between the storm and the thermospheric winds at these altitudes. The lower thermospheric zonal winds (95–200 km) in the 2 years show fewer differences. But a slight decrease in westward intensity is observed around 120-150 km during the hurricane by approximately  $10 \text{ m s}^{-1}$ . Around 100 km there is an indication of an increase in westward wind speed during the hurricane year although it is modest, by a couple tens of m s<sup>-1</sup>.

The thermospheric meridional winds exhibit more variability (panels e–h). A weak southward flow which later transitions to a stronger northward flow around 4 days after the date of intensification of the hurricane in 2021 is seen in the non-hurricane year, 2020 (panel e). The 2021 winds show an immediate reversal to slightly stronger northward flow, with speeds reaching up to 50 m s<sup>-1</sup> at approximately 200 km altitude, occurring right after the

21699402, 2024, 10, Down

https://agupubs.onlinelibrary.wiley.com/doi/10.1029/2024JA032933 by George Mason University, Wiley Online Library on [21/10/2024]. See the "

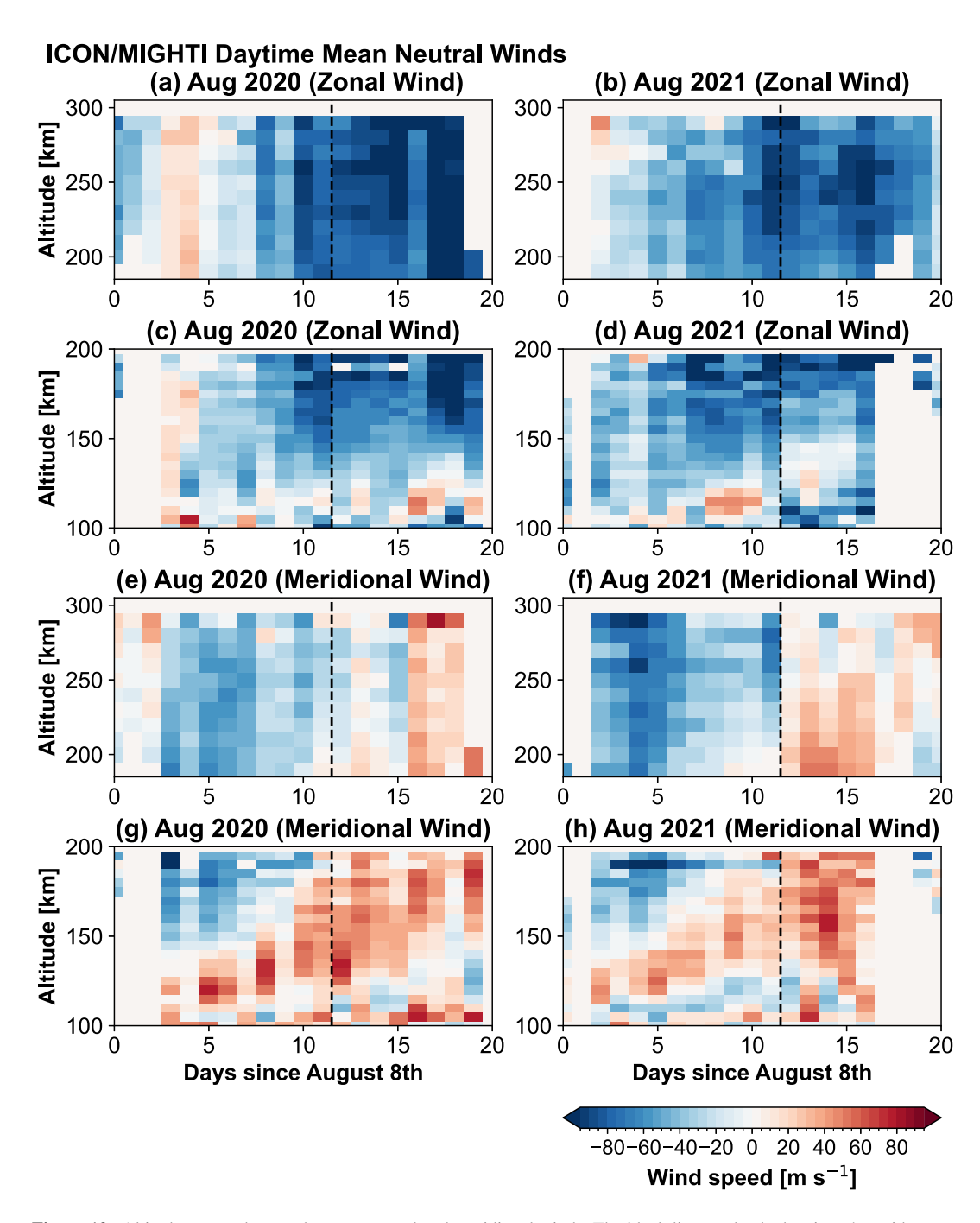


**Figure 12.** Altitude versus day number mean zonal and meridional winds. The black line marks the hurricane's rapid intensification on August 20th. It was constrained to latitudes 10° to 30°, longitudes 240° to 330°, and local time coverage from 7 to 17. Panels (a), (c), (e), and (g) show August 2020, while panels (b), (d), (f), and (h) show August 2021. Red line data is shown in panels (a), (b), (e), and (f). The data was binned into 5° altitude bins for the green line data, and 10° altitude bins for the red line data.

hurricane's peak intensity (panel f). The lower altitude comparison for the meridional wind (95–200 km) also show a difference (panels g, h). A northward flow increase to about  $65 \text{ m s}^{-1}$  is seen in the non-hurricane year (2020), which is not present in the hurricane year. Additionally, on the day of the hurricane's rapid intensification, there is an observable deceleration in the northward meridional wind, followed by an increase 2 and 3 days later. The observed change in meridional wind direction above 190 km after August 22 in both years likely reflects the seasonal transition of thermospheric circulation. It has been found that zonal-mean meridional winds in the

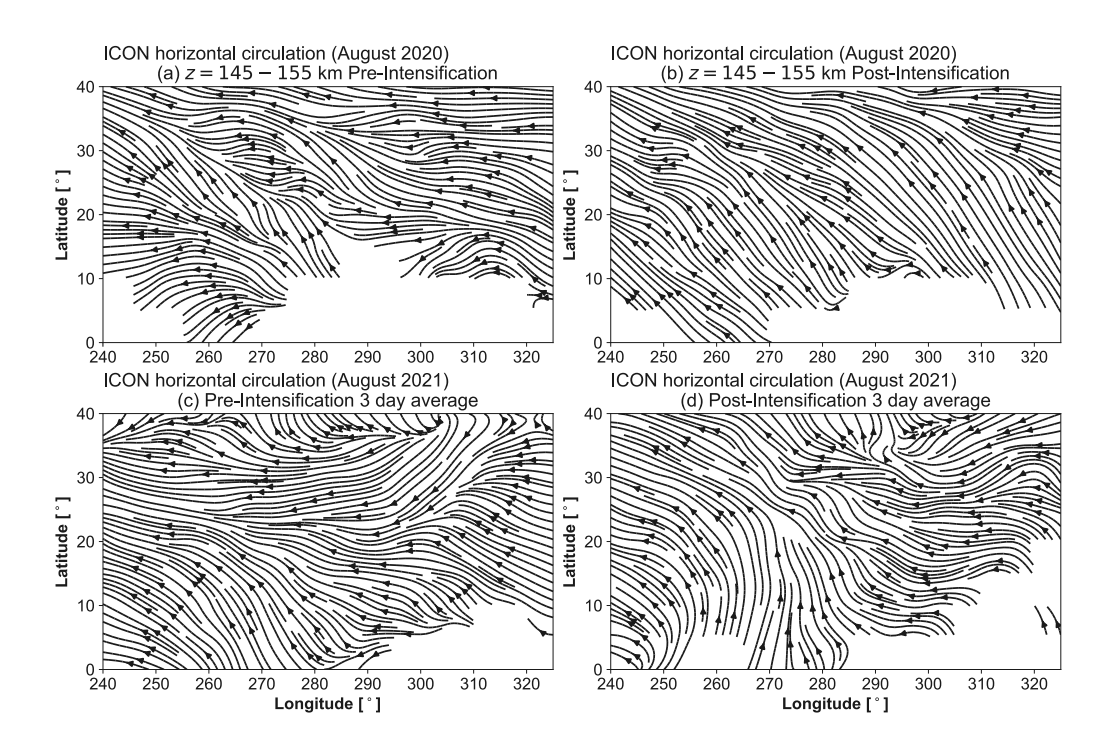


**Figure 13.** ICON horizontal circulation streamlines. ICON *u* and *v* wind components are calculated and plotted as streamlines for a Representative altitude band (145–155 km). Panels (a) and (c) show a 3 day average before intensification (16th, 17th, 18th), while panels (b) and (d) show a 3 day average during the rapid intensification (19th, 20th, and 21st). The top two panels (a) and (b) show the previous year and the bottom two panels (c) and (d) display data from the hurricane year.

middle thermosphere (200–300 km) typically shift from southward to northward flow in August and September (Yamazaki et al., 2023). The earlier reversal in 2021 coinciding with hurricane intensification suggests that while this is a primarily seasonal effect, the hurricane may have influenced the timing of the transition.

Figure 13 shows the 3-day mean horizontal circulation from ICON at an altitude of 145–155 km, depicted by streamlines from u and v wind components. This altitude range approximately matches GOLD measurements, which observed significant temperature increases during the hurricane. The top panels (a, b) present the non-hurricane year 2020, while the bottom ones (c, d) show the hurricane year 2021, before (August 16–18) and during (August 19–21) the rapid intensification. In the absence of the hurricane, westward and northwestward flows prevail, particularly in the pre-intensification phase of 2021 (panel c). During the intensification in 2021, significant changes occur: the westward flow is disrupted, especially between longitudes  $-100^{\circ}$  and  $-60^{\circ}$ , aligning with the hurricane's location. This disruption causes a pronounced northward shift in the horizontal flow across latitudes  $0^{\circ}$  to  $40^{\circ}$ N, demonstrating the hurricane's impact on thermospheric circulation.

In order to examine both magnitude and direction of circulation, we show the horizontal circulation in terms of vector winds. Figures 14-16 present vector winds at three representative altitudes (145-155 km, 175-185 km, and 215-225 km), respectively, in the same configuration as Figure 13. At 145-155 km, 2020 exhibits consistent westward and northwestward flow. In 2021, the pre-intensification phase shows a pronounced westward flow, while during intensification, this flow is disrupted, shifting northward, particularly between latitudes  $10^{\circ}$  and  $30^{\circ}$ N and longitudes  $-70^{\circ}$  and  $-100^{\circ}$ , exceeding 50 m s<sup>-1</sup> in magnitude.

At 175–185 km, non-hurricane years show dominant westward and northwestward flow with some southward turning at equatorial latitudes. In 2021, the pre-intensification phase is predominantly westward, but during intensification, there is a dramatic shift to northward flow at most latitudes, with an increase in wind speed in midlatitudes by up to a factor of 2 to 3. At 215–225 km, typical westward flow veers southwestward as latitude decreases. During pre-hurricane intensification in 2021, a southeast flow is observed, with stronger southwest flow toward the equator. During intensification, flow diminishes in magnitude and shifts to northwest, indicating the hurricane's influence extends to higher atmospheric levels. The consistent directional changes across altitudes suggest hurricanes profoundly impact over a wide range of altitudes in the thermosphere.



21699402, 2024, 10, Downlo

from https://agupubs.onlinelibrary.wiley.com/doi/10.1029/2024JA032933 by George Mason University, Wiley Online Library on [21/10/2024]. See the Terms

Figure 14. ICON horizontal circulation vectors. ICON u and v wind components are calculated and plotted as vectors for a Representative altitude band (145–155 km). Panels (a) and (c) show a 3 day average before intensification (16th, 17th, 18th), while panels (b) and (d) show a 3 day average during the rapid intensification (19th, 20th, and 21st). The top two panels (a) and (b) show the previous year and the bottom two panels (c) and (d) display data from the hurricane year. A scale arrow of  $50 \, \text{ms}^{-1}$  is provided.

To explore the extent of the hurricane's impact on circulation patterns we next examine how the average circulation angle above the hurricane changes as a function of altitude. Figure 17 shows the evolution of circulation angle with altitude using ICON u and v wind components (red line in the top panel and green line in the bottom panel) to calculate average angles in a  $10^{\circ} \times 10^{\circ}$  latitude-longitude bin near the hurricane's center on August 20. Wind vector angles indicate directional flow:  $0^{\circ}$  for eastward,  $90^{\circ}$  for northward,  $180^{\circ}$  for westward, and  $270^{\circ}$  for southward. The red and green line data are binned with different altitude intervals, 10 and 5 km, respectively. Data from 100 to 140 km show the largest magnitude of change between pre- and during rapid intensification. In general, the flows alternate between northwest and southwest directions. The top panel shows a more evident hurricane effect, indicating that effects extend up to 300 km. Figure 18 presents the standard deviation of the wind vector angle, indicating variability in wind direction across altitudes. While variability is generally similar across the four periods, an increase arises above 200 km during the 2021 intensification phase. Here, the standard deviation escalates to two to three times higher than the other periods, hinting at a marked increase in atmospheric disturbances. This heightened variability could be indicative of increased GW activity during the hurricane. The relation to gravity wave activity will be examined more comprehensively in the discussion section, yielding insights into the vertical coupling caused by tropical cyclones.

#### 4. Discussion

The data from COSMIC-2 during Hurricane Grace reveal pronounced variations in ionospheric electron density, particularly within the latitude and longitude ranges centered around the hurricane's center. The observed fluctuations in electron density, specifically the significant increases from around  $0.39 \times 10^6$  to  $1.06 \times 10^6$  cm<sup>-3</sup> around 295 km, are indicative of vertical coupling between the lower atmosphere affected by the hurricane and the ionosphere. Consistent with the findings of other studies of tropical cyclones (Bauer, 1958; Chou et al., 2017; W.

40°I

20°

10°I

40°N

30

0

Latitude

0

ICON Mean Horizontal Circulation (175-185 km) (a) 17-19 Aug 2020 (pre-Intensification)

80°W

(c) 17-19 Aug 2021 (pre-Intensification)

80°W

Longitude

60°W

100°W

100°W

80°W

80°W

Longitude

60°W

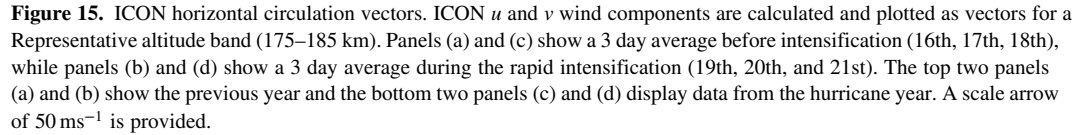
60°W

100°W

100°W

from https://agupubs.onlinelibrary.wiley.com/doi/10.1029/2024JA032933 by George Mason University, Wiley Online Library on [21/10/2024]. See the Term

21699402, 2024, 10, Down



40°W

40°1 30°1

20°l

10°1

40°N

30

20° 10°

0

40°W 50 ms<sup>-1</sup>

Li et al., 2017; Mao et al., 2010; Yang & Liu, 2016), these ionospheric responses may be attributed to the strong convective activity associated with Hurricane Grace.

Prior to Hurricane Grace, the electron density exhibited typical diurnal and spatial variations. During the hurricane, particularly during its rapid intensification and landfall on August 19th to 21st, we observed significant increases in electron density at altitudes between 200 and 380 km. This observed electron density enhancement strongly suggests a causal link between the hurricane's lower atmospheric activity and ionospheric disturbances.

The electron density enhancement and its spatial consistency within the hurricane's track strengthen the hypothesis that hurricanes can generate disturbances that propagate into the ionosphere, causing notable alterations in electron density. This is supported by previous studies suggesting that atmospheric transient events such as hurricanes can indeed lead to ionospheric disturbances (Perevalova & Ishin, 2011).

The electron density enhancements and changes in horizontal circulation during Hurricane Grace point to a substantial meteorological influence on the ionosphere, echoing the findings of several studies which have confirmed the ionosphere's susceptibility to lower atmospheric meteorological events (Kazimirovsky, 2003; Lin et al., 2012; Mao et al., 2010; Yang & Liu, 2016). The thermospheric warming of more than 50 K as observed by GOLD (Figures 10 and 11) around the time of the hurricane's rapid intensification suggests a strong thermodynamical coupling between the storm-time convective activity and thermospheric temperature. Strong changes in the horizontal circulation could modulate advective heat transport and affect the vertical circulation (upwelling/ downwelling), which can lead to the heating of the neutral gas.



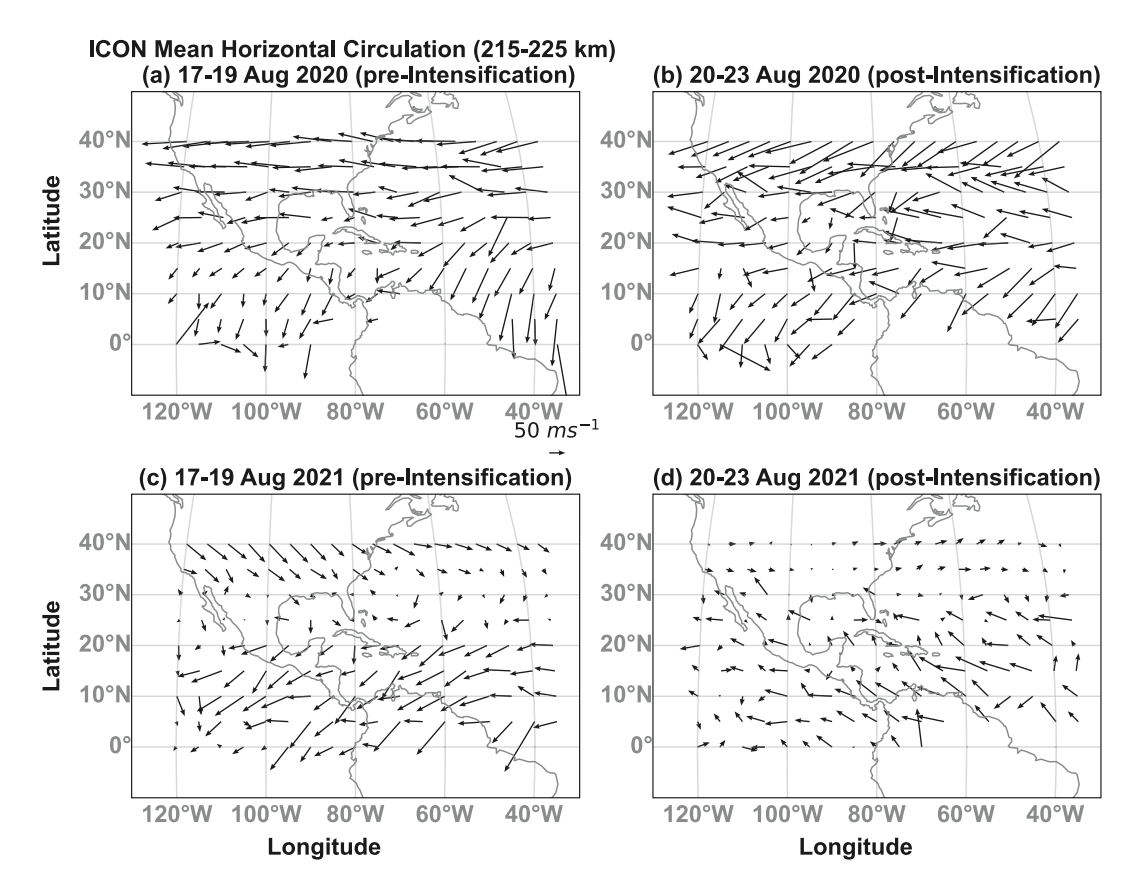


Figure 16. ICON horizontal circulation vectors. ICON u and v wind components are calculated and plotted as vectors for a Representative altitude band (215–225 km). Panels (a) and (c) show a 3 day average before intensification (16th, 17th, 18th), while panels (b) and (d) show a 3 day average during the rapid intensification (19th, 20th, and 21st). The top two panels (a) and (b) show the previous year and the bottom two panels (c) and (d) display data from the hurricane year. A scale arrow of  $50 \, \text{ms}^{-1}$  is provided.

The temperature increase of several tens of degrees observed around 150 km (Figure 9) could be attributed to several mechanisms associated with the hurricane's activity. The upward propagation and dissipation of gravity waves generated by the hurricane's intense convection could deposit energy at these altitudes leading to localized heating, as gravity waves can produce irreversible heating in the mesosphere and thermosphere (Gavrilov et al., 2020; Hickey et al., 2011; Yiğit & Medvedev, 2009). Hurricane-induced large-scale thermal and dynamical effects can alter the circulation throughout the lower and middle atmosphere, creating favorable propagation conditions for westward propagating GWs and potentially altering heat transport. These circulation changes can contribute to heating through increased downwelling at these latitudes. Additionally, storm-induced electric field perturbations could impact the thermosphere's energy balance through processes such as Joule heating. Modulation of the Joule heating of the thermospheric gas can occur via coupling of the ions to the changes in the motion of the neutrals (Yiğit & Ridley, 2011). As seen in Figure 1, the hurricane's wind speeds on August 18 and 19 were comparable to those observed on August 20 and 21. This consistency in the wind speeds along the hurricane's trajectory is reflected in the thermospheric temperature data. Figure 9 shows a slight increase of about 10–15 K in the region of 20–30°N on August 19, which aligns with the hurricane's position and intensity at that time.

The elevated thermospheric temperatures reported by GOLD in proximity to the hurricanes center are concurrent with the peak electron density enhancements in the ionosphere. The manifestation of thermospheric temperature gradients and deviations in wind patterns indicate an atmospheric perturbation extending upward from the hurricane, potentially related to changes in the turbopause altitude (Y. Liu et al., 2006). The significant divergence in wind vector angles post-intensification above 200 km altitude, as shown by the standard deviation increases (Figure 18), could be indicative of gravity wave activity (Q. Li et al., 2022).

21699402, 2024, 10, Downloaded from https://agupubs.onlinelibrary.wiley.com/doi/10.1029/2024/A032933 by George Mason University, Wiley Online Library on [21/10/2024]. See the Terms

Figure 17. ICON evolution of horizontal wind vector angle with altitude. The data is taken from a  $10^{\circ} \times 10^{\circ}$  bin around the hurricane's center, latitudes  $15^{\circ}$ – $25^{\circ}$  and longitudes  $290^{\circ}$ – $300^{\circ}$ .  $0^{\circ}$  vector angle represents eastward flow,  $90^{\circ}$  represents northward flow,  $180^{\circ}$  is westward, and  $270^{\circ}$  is southward. The top panel is red line data while the bottom is green line data. Data points are plotted as a scatter plot and a dashed line connects the means of each angle for each altitude level. Red line data has  $10^{\circ}$  altitude intervals and green line data has  $5^{\circ}$  altitude intervals. Blue lines and marks indicate 2020 3 days pre-intensification, red indicates 2020 post-intensification, green represents 2021 pre-intensification, and yellow represents 2021 post-intensification.

The connection between hurricane activity and ionospheric electron density is a complex nonlinear long-range coupling. While we observed overall increases in electron density during Hurricane Grace's intensification, both increases and decreases in  $F_2$  layer electron concentration are possible during such transient events. The observed changes could follow a sequence initiated by GWs, with GW propagation and dissipation first causing changes in temperature, which then leads to alterations in wind amplitude. These wind changes can subsequently affect the distribution of gas components in the thermosphere, particularly the  $O/N_2$  ratio. This chain of events

21699402, 2024, 10, Downloaded

from https://aguputs.onlinelibrary.wiley.com/doi/10.1029/2024JA032933 by George Mason University, Wiley Online Library on [21/10/2024]. See the Terms from https://aguputs.onlinelibrary.wiley.com/doi/10.1029/2024JA032933 by George Mason University, Wiley Online Library on [21/10/2024].

**Figure 18.** ICON horizontal wind vector angle standard deviation as a function of altitude. Blue lines and marks indicate 2020 3 days pre-intensification, red indicates 2020 post-intensification, green represents 2021 pre-intensification, and yellow represents 2021 post-intensification.

can trigger the occurrence of traveling ionospheric disturbances (TIDs) and ultimately result in changes to the electron density of the ionosphere. The observed effects depend on the interconnection of these processes and the relative position of the observation area to the storm. Additional factors contributing to ionospheric effects could include temperature increases (and subsequent expansion) above the hurricane area effecting recombination rates, and plasma transfer processes from regions of large-scale thermospheric disturbances (Karpov et al., 2019).

The dissipation of atmospheric tides in the lower thermosphere drives a mean meridional circulation, increasing the downward transport of atomic oxygen, leading to greater loss of this species at lower altitudes (Yamazaki & Richmond, 2013). This suggests that changes in lower thermospheric circulation due to tidal dissipation has significant effects on the distribution of the  $O/N_2$  ratio. However, gravity waves modulate the diurnal and the

semidiurnal tides throughout the mesosphere and thermosphere (Manson et al., 1998; Miyoshi & Yiğit, 2019; Yiğit & Medvedev, 2017) and it is yet to be modeled how such wave-wave interactions modulate downward transport of atomic oxygen. In the context of hurricane-generated gravity waves, it is possible that gravity waves could induce similar circulation changes via wave-mean flow interactions, potentially competing with or even dominating over those produced by turbulent diffusion in the mesosphere and lower thermosphere. Gravity waves can modify the circulation, which in turn modulates upwelling and downwelling. These gravity wave-induced circulation changes can affect thermospheric composition causing interhemispheric flow from summer to winter under the influence of the Coriolis force, resulting in variations in vertical motion (Qian et al., 2009). While previous studies focused on seasonal variations, hurricane-generated gravity waves could cause intense circulation changes, leading to vertical motions that affect the O/N2 ratio. However, the complexity of the observed changes during Hurricane Grace suggests that multiple mechanisms may be occurring simultaneously in a nonlinear fashion and producing the dramatic short-term variations. An accurate assessment of the relative importance of these processes in changing the O/N2 ratio requires detailed global-scale modeling efforts that couple the large-scale circulation, subgrid-scale gravity waves, tidal dissipation, and composition. However, there are still uncertainties with quantifying these effects, as global models still heavily rely on parameterizations of subgrid-scale processes (e.g., turbulent diffusion, gravity waves) that are not fully constrained by observations.

We observed a great deal of ionospheric variability during the influence of Hurricane Grace. Ionospheric variability on daily timescales can be influenced by lower atmospheric phenomena. The ionospheric dynamo mechanism serves as a link in this vertical coupling process, translating atmospheric wave activity into perturbations of ionospheric electric fields and currents (Jin, 2009). In the case of intense tropospheric events like Hurricane Grace, this coupling mechanism may play a key role in transmitting storm-induced disturbances to ionospheric heights, potentially modifying the ambient electrodynamics of the upper atmosphere. The circulation changes observed by ICON during Hurricane Grace, especially those extending up to the E-region altitudes, could modify the ionospheric dynamo. Neutral winds in this region drive currents that generate electric fields (Richmond et al., 1976). Altered wind patterns near the Hall and Pedersen conductivity peaks could change the typical dynamo electric fields, potentially leading to modifications in F-region electron densities through changes in E × B drifts (Jin, 2009). Additionally, if the hurricane-induced circulation changes modify the dynamo electric field, it could alter the strength or structure of the Equatorial Ionization Anomaly (EIA) (Maute et al., 2012). This could explain some of the observed changes in F-region electron density. In the context of geomagnetic storms, the low latitude ionosphere has been observed to be positively charged due to Pedersen and Hall currents caused by westward and equatorward neutral disturbances (Huang, 2013). This principle of wind-driven changes in electric field could apply to Hurricane Grace. While the dynamo mechanism provides a plausible explanation for some of the observed ionospheric changes, it likely interacts with other hurricane-induced disturbances, such as gravity waves, leading to complex spatiotemporal patterns in ionospheric variability. However, attributing these effects solely to dynamo processes has limitations due to the ionosphere's complexity and the influence of various factors including solar and geomagnetic activity. The non-linear nature of ionospheric processes suggests that the observed effects may result from a combination of mechanisms rather than a single dominant process.

#### 5. Summary and Conclusions

This paper presented a detailed investigation into the upper atmospheric effects of the 2021 Hurricane Grace, as observed by COSMIC-2, ICON, and GOLD satellites.

The main inferences of this study are as follows:

- 1. Hurricane Grace induced perturbations in the ionospheric electron density, likely due to the dynamic coupling with the lower atmosphere enhanced by the hurricane's convective activity.
- 2. Thermospheric temperatures around the hurricane's rapid intensification showed a warming of more than 50 K, which was consistently seen in GOLD observations.
- 3. Substantial deviations from typical thermospheric wind patterns were observed by ICON during the hurricane, with circulation changes extending from the lower thermosphere up to 300 km.
- 4. The observed thermospheric warming and alterations in thermospheric circulation and ionospheric electron density provide compelling evidence of the involvement of gravity waves in vertical coupling during hurricanes.



21699402, 2024, 10, Downlo

loi/10.1029/2024JA032933 by George Mason University, Wiley Online Library on [21/10/2024]. See the T

This study shows the importance of atmospheric remote-sensing to better characterize the coupling between Earth's atmospheric layers. There is a need for continued and enhanced satellite monitoring of the upper atmosphere to better understand the temporal and spatial scales of hurricane-induced disturbances. The detailed investigation of the thermospheric and ionospheric effects of hurricanes requires global-scale modeling efforts that interactively couple the neutral and plasma processes with small-scale gravity wave generation, propagation, and dissipation. The advancement of our capabilities to model and observe these complex coupling interactions will help mitigate the adverse effects on our society.

The findings presented reinforce the concept that meteorological processes are now recognized as vital contributors to ionospheric and thermospheric variability (Kazimirovsky, 2003). The disruptions in the ionosphere and thermosphere observed during Hurricane Grace's intensification period are consistent with the theory that significant meteorological events can induce far-reaching atmospheric changes. This study highlights the need for dedicated modeling and observational studies of hurricane-induced high altitude effects.

#### **Data Availability Statement**

The data on which this article is based are available in the following data sets: COSMIC-2 electron density profiles (CDAAC, 2019) Available via: COSMIC Data Analysis and Archive Center URL: https://doi.org/10.5065/t353-c093. ICON/MIGHTI horizontal wind data (version 5) (Immel et al., 2018a, 2018b) Available via: ICON data center URL: https://icon.ssl.berkeley.edu/Data. GOLD level 2 data (Eastes et al., 2020a, 2020b) Available via: GOLD Science Data Center and NASA's Space Physics Data Facility URL: https://gold.cs.ucf.edu/search/. MERRA-2 data (GMAO, 2015) Available from: Global Modeling and Assimilation Office Access: Freely accessible with registration required URL: https://doi.org/10.5067/0TUFO90Q2PMS. Hurricane path data (National Hurricane Center, 2023) Available from: National Hurricane Center URL: https://www.nhc.noaa.gov/data/. The figures in this article were created using the following software: Matplotlib version 3.7.2 (Caswell et al., 2023) Available from: Zenodo Access: Freely accessible under the Matplotlib license URL: https://doi.org/10.5281/zenodo.8118151. The software is also available at https://matplotlib.org/. All data sets are provided in standard scientific formats (e.g., NetCDF, CSV) and are accompanied by metadata describing the variables and units. The software used for data analysis and figure creation is open-source and freely available.

### Acknowledgments

This work was supported by NASA (Grant 80NSSC22K0016) and National Science Foundation (Grant AGS 2330046). Thank you to Md Nazmus Sakib for advice and providing some code for the COSMIC-2 data.

#### References

- Amayenc, P., & Vasseur, G. (1972). Neutral winds deduced from incoherent scatter observations and their theoretical interpretation. *Journal of Atmospheric and Terrestrial Physics*, 34(3), 351–364. https://doi.org/10.1016/0021-9169(72)90038-4
- Anthes, R., & Schreiner, W. (2019). Six new satellites watch the atmosphere over Earth's equator. Eos, 100. https://doi.org/10.1029/2019E0131779
- Ashneel, S. (2022). Analyzing the effects of tropical cyclone on critical frequency of the F 2-region ionosphere in South Pacific Region. Geomagnetism and Aeronomy, 62(1), S128–S141. https://doi.org/10.1134/S0016793222600175
- Bao, J., Wilczak, J., Choi, J., & Kantha, L. (2000). Numerical simulations of air-sea interaction under high wind conditions using a coupled model:

  A study of hurricane development. *Monthly Weather Review*, 128(7), 2190–2210. https://doi.org/10.1175/1520-0493(2000)128(2190: NSOASI)2.0.CO:2
- Bauer, S. J. (1958). An apparent ionospheric response to the passage of hurricanes. *Journal of Geophysical Research*, 63(1), 265–269. https://doi.org/10.1029/JZ063i001p00265
- Beven, J. L. (2021). The 2020 Atlantic hurricane season: The most active season on record. Weatherwise, 74(5), 33–43. https://doi.org/10.1080/00431672.2021.1953905
- Borchevkina, O., Karpov, I., & Karpov, M. (2020). Meteorological storm influence on the ionosphere parameters. *Atmosphere*, 11(9), 1017. https://doi.org/10.3390/atmos11091017
- Brad, J., Reinhart, R. B., & Amanda, R. (2022). National hurricane center tropical cyclone report: Hurricane grace (Vol. 49). National Hurricane Center. Retrieved from https://www.nhc.noaa.gov/data/tcr/AL072021\_Grace.pdf
- Caswell, T. A., Sales de Andrade, E., Lee, A., Droettboom, M., Hoffmann, T., Klymak, J., et al. (2023). Matplotlib v3.7.2 Zenodo [Software].
  Zenodo. https://doi.org/10.5281/zenodo.8118151
- CDAAC. (2019). COSMIC-2 electron density profiles [Dataset]. COSMIC Data Analysis and Archive Center. https://doi.org/10.5065/t353-c093
  Chernogor, L. F. (2023). A tropical cyclone or typhoon as an element of the Earth–atmosphere–ionosphere–magnetosphere system: Theory, simulations, and observations. Remote Sensing, 15(20), 4919. https://doi.org/10.3390/rs15204919
- Chou, M. Y., Lin, C. C. H., Yue, J., Tsai, H. F., Sun, Y. Y., Liu, J. Y., & Chen, C. H. (2017). Concentric traveling ionosphere disturbances triggered by Super Typhoon Meranti (2016). *Geophysical Research Letters*, 44(3), 1219–1226. https://doi.org/10.1002/2016GL072205
- Cotton, W. R., & Walko, R. (2021). A modeling investigation of the potential impacts of pollution aerosols on Hurricane Harvey. *Journal of the Atmospheric Sciences*. https://doi.org/10.1175/jas-d-20-0076.1
- Davis, N. A., Richter, J. H., Glanville, A. A., Edwards, J., & LaJoie, E. (2022). Limited surface impacts of the January 2021 sudden stratospheric warming. *Nature Communications*, 13(1), 1136. https://doi.org/10.1038/s41467-022-28836-1
- Dewan, E. M., Picard, R. H., O'Neil, R. R., Gardiner, H. A., Gibson, J., Mill, J. D., et al. (1998). Msx satellite observations of thunder-stormgenerated gravity waves in midwave infrared images of the upper stratosphere. *Geophysical Research Letters*, 25(7), 939–942. https://doi.org/10.1029/98g100640

- Eastes, R. W., McClintock, W. E., Burns, A. G., Anderson, D. N., Anderson, L., Aryal, S., et al. (2020b). Initial observations by the GOLD mission. *Journal of Geophysical Research: Space Physics*, 125(7), e2020JA027823. https://doi.org/10.1029/2020JA027823
- Eastes, R. W., McClintock, W. E., Burns, A. G., Anderson, D. N., Andersson, L., Codrescu, M., et al. (2017). The global-scale observations of the limb and disk (GOLD) mission. Space Science Reviews, 212(1), 383–408. https://doi.org/10.1007/s11214-017-0392-2
- Eastes, R. W., McClintock, W. E., Burns, A. G., Anderson, D. N., Anderson, L., Codrescu, M., et al. (2020a). Global-scale observations of the limb and disk (GOLD) mission level 2 data [Dataset]. GOLD Science Data Center. Retrieved from https://gold.cs.ucf.edu/search/
- Englert, C. R., Harlander, J. M., Brown, C. M., Marr, K. D., Miller, I. J., Stump, J. E., et al. (2017). Michelson interferometer for global high-resolution thermospheric imaging (MIGHTI): Instrument design and calibration. Space Science Reviews, 212(1–2), 553–584. https://doi.org/10.1007/s11214-017-0358-4
- Ezer, T. (2019). Numerical modeling of the impact of hurricanes on ocean dynamics: Sensitivity of the Gulf Stream response to storm's track. *Ocean Dynamics*, 69(9), 1053–1066. https://doi.org/10.1007/s10236-019-01289-9
- Feng, J., & Wang, X. (2019). Impact of assimilating upper-level dropsonde observations collected during the TCI field campaign on the prediction of intensity and structure of Hurricane Patricia (2015). Monthly Weather Review, 147(8), 3069–3089. https://doi.org/10.1175/mwr-d-18-0305.1
- Fong, C.-J., Chu, C.-H., Lin, C.-L., & Curiel, A. D. S. (2019). Toward the most accurate thermometer in space: FORMOSAT-7/COSMIC-2 constellation. IEEE Aerospace and Electronic Systems Magazine, 34(8), 12–20. https://doi.org/10.1109/MAES.2019.2924133
- Forbes, J. M., Oberheide, J., Zhang, X., Cullens, C., Englert, C. R., Harding, B. J., et al. (2022). Vertical coupling by solar semidiumnal tides in the thermosphere from ICON/MIGHTI measurements. *Journal of Geophysical Research: Space Physics*, 127(5), e2022JA030288. https://doi.org/ 10.1029/2022JA030288
- Foti, G., Gommenginger, C., & Srokosz, M. (2017). First Spaceborne GNSSReflectometry observations of hurricanes from the UK TechDemoSat1 mission. Geophysical Research Letters, 44(24). https://doi.org/10.1002/2017gl076166
- Fritts, D. C., & Alexander, M. J. (2003). Gravity wave dynamics and effects in the middle atmosphere. Reviews of Geophysics, 64(1). https://doi.org/10.1029/2001rg000106
- Fritts, R. (2020). To make better hurricane models. Consider Air Pollution. Eos, 101. https://doi.org/10.1029/2020eo153044
- Gasperini, F., Harding, B. J., Crowley, G., & Immel, T. J. (2023). Ionosphere-thermosphere coupling via global-scale waves: New insights from two-years of concurrent in situ and remotely-sensed satellite observations. Frontiers in Astronomy and Space Sciences, 10. https://doi.org/10. 3389/fspas.2023.1217737
- Gavrilov, N. M., Kshevetskii, S. P., & Koval, A. V. (2020). Thermal effects of nonlinear acoustic-gravity waves propagating at thermospheric temperatures matching high and low solar activity. *Journal of Atmospheric and Solar-Terrestrial Physics*, 208, 105381. https://doi.org/10. 1016/j.jastp.2020.105381
- Geernaert, G. L., Larsen, S. E., & Hansen, F. (1987). Measurements of the wind stress, heat flux, and turbulence intensity during storm conditions over the North Sea. *Journal of Geophysical Research*, 92(C12), 13127–13139. https://doi.org/10.1029/jc092ic12p13127
- GMAO. (2015). MERRA-2 tavg33dmstNp: 3d, 3-Hourly, Time-Averaged, Pressure-Level, Assimilation, Moist processes diagnostics V5.12.4 [Dataset]. Goddard Earth Sciences Data and Information Services Center (GES DISC). https://doi.org/10.5067/0TUFO90Q2PMS
- Guha, A., Paul, B., Chakraborty, M., & De, B. K. (2016). Tropical cyclone effects on the equatorial ionosphere: First result from the Indian sector. Journal of Geophysical Research: Space Physics, 121(6), 5764–5777. https://doi.org/10.1002/2016JA022363
- Harding, B. J., Chau, J. L., He, M., Englert, C. R., Harlander, J. M., Marr, K. D., et al. (2021). Validation of ICON-MIGHTI thermospheric wind observations: 2. Green-line comparisons to specular meteor radars. *Journal of Geophysical Research: Space Physics*, 126(3), e2020JA028947. https://doi.org/10.1029/2020JA028947
- Hickey, M. P., Schubert, G., & Walterscheid, R. L. (2009). Propagation of tsunami-driven gravity waves into the thermosphere and ionosphere. Journal of Geophysical Research, 114(A8). https://doi.org/10.1029/2009JA014105
- Hickey, M. P., Walterscheid, R. L., & Schubert, G. (2011). Gravity wave heating and cooling of the thermosphere: Sensible heat flux and viscous flux of kinetic energy. *Journal of Geophysical Research*, 116(A12). https://doi.org/10.1029/2011JA016792
- Hordyniec, P., Kuleshov, Y., Choy, S., & Norman, R. (2022). Observation of deep occultation signals in tropical cyclones with COSMIC-2 measurements. *IEEE Geoscience and Remote Sensing Letters*, 19, 1–5. https://doi.org/10.1109/lgrs.2021.3092511
- Hristova-Veleva, S. M., Li, P. P., Knosp, B., Vu, Q., Turk, F. J., Poulsen, W. L., et al. (2020). An eye on the storm: Integrating a wealth of data for quickly advancing the physical understanding and forecasting of tropical cyclones. *Bulletin of the American Meteorological Society*, 101(10), E1718–E1742. https://doi.org/10.1175/bams-d-19-0020.1
- Huang, C. M. (2013). Disturbance dynamo electric fields in response to geomagnetic storms occurring at different universal times. *Journal of Geophysical Research: Space Physics*, 118(1), 496–501. https://doi.org/10.1029/2012JA018118
- Hung, R. (1981). Ionospheric observation of enhanced convection-initiated gravity waves during tornadic storms (Contract Report No. 3419)
  Huntsville, Alabama: NASA Contractor Report. Contract NAS8-31171, prepared for Marshall Space Flight Center. Marshall Space Flight Center.
- Hung, R., & Smith, R. (1978). Ionospheric and satellite observations for studying the dynamic behavior of typhoons and the detection of severe storms and tsunamis. In *International symposium on remote sensing of environment*. National Research Council of Canada. Quebec Department of Education, Universite de Sherbrooke. Document ID: 19790038654, Acquisition Source: Legacy CDMS, Accession Number: 79A22667, Distribution Limits: Public, Funding Number(s): NAS8-31171, NSF ATM-75-15706.
- Hung, R., & Smith, R. (1981). Infrared digital data analysis of severe storms and hurricanes from geosynchronous satellite. In *Proceedings of the international symposium on remote sensing of environment*. National Research Council of Canada. Quebec Department of Education, Universite de Sherbrooke. Document ID: 19820044081, Acquisition Source: Legacy CDMS, Accession Number: 82A27616, Distribution Limits: Public, Funding Number(s): NAS8-33726.
- Immel, T. J., England, S. L., Mende, S. B., Heelis, R. A., Englert, C. R., Edelstein, J., et al. (2018a). ICON/MIGHTI horizontal wind data (version 5) [Dataset]. ICON Data Center. Retrieved from https://icon.ssl.berkeley.edu/Data
- Immel, T. J., England, S. L., Mende, S. B., Heelis, R. A., Englert, C. R., Edelstein, J., et al. (2018b). The ionospheric connection explorer mission: Mission goals and design. Space Science Reviews, 214(1), 13. https://doi.org/10.1007/s11214-017-0449-2
- Jin, H. (2009). Ionospheric dynamo process. Journal of the National Institute of Information and Communications Technology, 56(1–4), 209–220.
  Karpov, I. V., Borchevkina, O. P., & Karpov, M. I. (2019). Local and regional ionospheric disturbances during meteorological disturbances.
  Geomagnetism and Aeronomy, 59(4), 458–466. https://doi.org/10.1134/S0016793219040108
- Kazimirovsky, E. (2003). Effects on the Ionosphere Due to Phenomena Occurring Below it. Surveys in Geophysics, 24(2), 139–184. https://doi.org/10.1023/A:1023206426746
- Koucká Knížová, P., Laštovička, J., Kouba, D., Mošna, Z., Podolská, K., Potužníková, K., et al. (2021). Ionosphere influenced from lower-lying atmospheric regions. Frontiers in Astronomy and Space Sciences, 8. https://doi.org/10.3389/fspas.2021.651445





# Journal of Geophysical Research: Space Physics

- 10.1029/2024JA032933
- Koucká Knížová, P., Podolská, K., Potužníková, K., Kouba, D., Mošna, Z., Boška, J., & Kozubek, M. (2020). Evidence of vertical coupling: Meteorological storm Fabienne on 23 September 2018 and its related effects observed up to the ionosphere. *Annales Geophysicae*, 38(1), 73–93. https://doi.org/10.5194/angeo-38-73-2020
- Kuester, M. A., Alexander, M. J., & Ray, E. A. (2008). A model study of gravity waves over Hurricane Humberto (2001). Journal of the Atmospheric Sciences, 65(10), 3231–3246. https://doi.org/10.1175/2008JAS2372.1
- Kurdyaeva, Y., Bessarab, F., Borchevkina, O., & Klimenko, M. (2024). Model study of the influence of atmospheric waves on variations of upper atmosphere and ionosphere parameters during a meteorological storm on May 29, 2017. Advances in Space Research, 74(5), 2463–2474. https://doi.org/10.1016/j.asr.2024.05.062
- Li, J., Li, J., Velden, C., Wang, P., Schmit, T. J., & Sippel, J. (2020). Impact of RapidScanBased dynamical information from GOES16 on HWRF hurricane forecasts. *Journal of Geophysical Research: Atmospheres*, 125(3). https://doi.org/10.1029/2019jd031647
- Li, Q., Xu, J., Liu, H., Liu, X., & Yuan, W. (2022). How do gravity waves triggered by a typhoon propagate from the troposphere to the upper atmosphere? *Atmospheric Chemistry and Physics*, 22(18), 12077–12091. https://doi.org/10.5194/acp-22-12077-2022
- Li, W., Yue, J., Yang, Y., Li, Z., Guo, J., Pan, Y., & Zhang, K. (2017). Analysis of ionospheric disturbances associated with powerful cyclones in East Asia and North America. *Journal of Atmospheric and Solar-Terrestrial Physics*, 161, 43–54. https://doi.org/10.1016/j.jastp.2017.06.012
- Lin, J. T., Lin, C. H., Chang, L. C., Huang, H. H., Liu, J. Y., Chen, A. B., et al. (2012). Observational evidence of ionospheric migrating tide modification during the 2009 stratospheric sudden warming. *Geophysical Research Letters*, 39(2), 2011GL050248. https://doi.org/10.1029/2011GL050248
- Liu, J.-Y., Lin, C.-H., Rajesh, P. K., Lin, C.-Y., Chang, F.-Y., Lee, I.-T., et al. (2022). Advances in ionospheric space weather by using FOR-MOSAT-7/COSMIC-2 GNSS radio occultations. Atmosphere, 13(6), 858. https://doi.org/10.3390/atmos13060858
- Liu, Y., Wang, J., Xiao, Z., & Suo, Y. (2006). A possible mechanism of typhoon effects on the ionospheric F2 layer. Chinese Journal of Space Science, 26(2), 92–97. https://doi.org/10.11728/ciss2006.02.092
- Manson, A., Meek, C., & Hall, G. (1998). Correlations of gravity waves and tides in the mesosphere over Saskatoon. *Journal of Atmospheric and Solar-Terrestrial Physics*, 60(11), 1089–1107. https://doi.org/10.1016/S1364-6826(98)00059-5
- Mao, T., Wang, J., Yang, G., Yu, T., Ping, J., & Suo, Y. (2010). Effects of typhoon Matsa on ionospheric TEC. Chinese Science Bulletin, 55(8), 712–717. https://doi.org/10.1007/s11434-009-0472-0
- Martines-Bedenko, V., Pilipenko, V., Zakharov, V., & Grushin, V. (2019). Influence of the Vongfong 2014 hurricane on the ionosphere and geomagnetic field as detected by SWARM satellites: 2. Geomagnetic disturbances. *Solnechno-Zemnaya Fizika*, 5(4), 90–98. https://doi.org/10.12737/szf-54201910
- Maute, A., Richmond, A. D., & Roble, R. G. (2012). Sources of low-latitude ionospheric E × B drifts and their variability. *Journal of Geophysical Research*, 117(A6), A06312. https://doi.org/10.1029/2011JA017502
- Medvedev, A. S., Klaassen, G. P., & Yiğit, E. (2023). On the dynamical importance of gravity wave sources distributed over different heights in the atmosphere. *Journal of Geophysical Research: Space Physics*, 128(3), e2022JA031152. https://doi.org/10.1029/2022JA031152
- Medvedev, A. S., Yiğit, E., & Hartogh, P. (2017). Ion friction and quantification of the geomagnetic influence on gravity wave propagation and dissipation in the thermosphere-ionosphere. *Journal of Geophysical Research: Space Physics*, 122(12), 12464–12475. https://doi.org/10.1002/
- Méndez-Tejeda, R., & Hernández-Ayala, J. J. (2023). Links between climate change and hurricanes in the North Atlantic. *PLOS Climate*, 2(4), e0000186. https://doi.org/10.1371/journal.pclm.0000186
- Mendillo, M., & Klobuchar, J. A. (2006). Total electron content: Synthesis of past storm studies and needed future work. *Radio Science*, 41(5). https://doi.org/10.1029/2005rs003394
- Miller, W. J., Chen, Y., Ho, S.-P., & Shao, X. (2023). Evaluating the impacts of COSMIC-2 GNSS RO bending angle assimilation on Atlantic hurricane forecasts using the HWRF model. *Monthly Weather Review*, 151(7), 1821–1847. https://doi.org/10.1175/mwr-d-22-0198.1
- Miyoshi, Y., & Yiğit, E. (2019). Impact of gravity wave drag on the thermospheric circulation: Implementation of a nonlinear gravity wave parameterization in a whole-atmosphere model. *Annales Geophysicae*. 37(5), 955–969. https://doi.org/10.5194/angeo-37-955-2019
- National Hurricane Center. (2023). Hurricane path data [Dataset]. National Hurricane Center. Retrieved from https://www.nhc.noaa.gov/data/Nolan, D. S., & Zhang, J. A. (2017). Spiral gravity waves radiating from tropical cyclones. Geophysical Research Letters, 44(8), 3924–3931. https://doi.org/10.1002/2017GL073572
- Pedatella, N. (2022). Ionospheric variability during the 2020–2021 SSW: COSMIC-2 observations and WACCM-X simulations. *Atmosphere*, 13(3), 368. https://doi.org/10.3390/atmos13030368
- Pedatella, N. M., Zakharenkova, I., Braun, J. J., Cherniak, I., Hunt, D., Schreiner, W. S., et al. (2023). Processing and validation of FORMOSAT-7/COSMIC-2 GLONASS total electron content observations. *Radio Science*, 58(6), e2022RS007589. https://doi.org/10.1029/2022RS007589
- Perevalova, N. P., & Ishin, A. B. (2011). Effects of tropical cyclones in the ionosphere from data of sounding by GPS signals. *Izvestiya Atmospheric and Oceanic Physics*, 47(9), 1072–1083. https://doi.org/10.1134/S000143381109012X
- Polyakova, A., & Perevalova, N. (2011). Investigation into impact of tropical cyclones on the ionosphere using GPS sounding and NCEP/NCAR Reanalysis data. Advances in Space Research, 48(7), 1196–1210. https://doi.org/10.1016/j.asr.2011.06.014
- Qian, L., Solomon, S. C., & Kane, T. J. (2009). Seasonal variation of thermospheric density and composition: Seasonal variation of the thermosphere. *Journal of Geophysical Research*, 114(A1). https://doi.org/10.1029/2008JA013643
- Richmond, A. D., Matsushita, S., & Tarpley, J. D. (1976). On the production mechanism of electric currents and fields in the ionosphere. *Journal of Geophysical Research*, 81(4), 547–555. https://doi.org/10.1029/JA081i004p00547
- Snively, J. B., Sabatini, R., Calhoun, D. A., Heale, C. J., Inchin, P. A., & Zettergren, M. D. (2022). Modeling of acoustic and gravity wave interactions, coupling, and observables above meteorological systems. *Journal of the Acoustical Society of America*, 151(4\_Supplement), A161. https://doi.org/10.1121/10.0010975
- Stettner, D., Velden, C., Rabin, R., Wanzong, S., Daniels, J., & Bresky, W. (2019). Development of enhanced vortex-scale atmospheric motion vectors for hurricane applications. *Remote Sensing*, 11(17), 1981. https://doi.org/10.3390/rs11171981
- Tratt, D. M., Hackwell, J. A., Valant-Spaight, B. L., Walterscheid, R. L., Gelinas, L. J., Hecht, J. H., et al. (2018). GHOST: A satellite mission concept for persistent monitoring of stratospheric gravity waves induced by severe storms. Bulletin of the American Meteorological Society, 99(9), 1813–1828. https://doi.org/10.1175/BAMS-D-17-0064.1
- Venkatesh, K., Rama Rao, P. V. S., Prasad, D. S. V. V. D., Niranjan, K., & Saranya, P. L. (2011). Study of TEC, slab-thickness and neutral temperature of the thermosphere in the Indian low latitude sector. *Annales Geophysicae*, 29(9), 1635–1645. https://doi.org/10.5194/angeo-29-1635-2011
- Wright, C. J. (2019). Quantifying the global impact of tropical cycloneassociated gravity waves using HIRDLS, MLS, SABER and IBTrACS data. Quarterly Journal of the Royal Meteorological Society, 145(724), 3023–3039. https://doi.org/10.1002/qj.3602





# Journal of Geophysical Research: Space Physics

- 10.1029/2024JA032933
- Wu, X., Hoffmann, L., Wright, C. J., Hindley, N. P., Kalisch, S., Alexander, M. J., & Wang, Y. (2021). Stratospheric gravity waves as a proxy for hurricane intensification: A case study of weather research and forecast simulation for Hurricane Joaquin. Geophysical Research Letters, 49(1). https://doi.org/10.1029/2021g1097010
- Xu, S., Yue, J., Xue, X., Vadas, S. L., Miller, S. D., Azeem, I., et al. (2019). Dynamical coupling between Hurricane Matthew and the middle to upper atmosphere via gravity waves. *Journal of Geophysical Research: Space Physics*, 124(5), 3589–3608. https://doi.org/10.1029/20181A026453
- Yamazaki, Y., Harding, B. J., Qiu, L., Stolle, C., Siddiqui, T. A., Miyoshi, Y., et al. (2023). Monthly climatologies of zonal-mean and tidal winds in the thermosphere as observed by ICON/MIGHTI during April 2020–March 2022. Earth and Space Science, 10(6), e2023EA002962. https://doi.org/10.1029/2023EA002962
- Yamazaki, Y., & Richmond, A. D. (2013). A theory of ionospheric response to upward-propagating tides: Electrodynamic effects and tidal mixing effects. *Journal of Geophysical Research: Space Physics*, 118(9), 5891–5905. https://doi.org/10.1002/jgra.50487
- Yang, Z., & Liu, Z. (2016). Observational study of ionospheric irregularities and GPS scintillations associated with the 2012 tropical cyclone Tembin passing Hong Kong. *Journal of Geophysical Research: Space Physics*, 121(5), 4705–4717. https://doi.org/10.1002/2016JA022398
- Yiğit, E., Aylward, A. D., & Medvedev, A. S. (2008). Parameterization of the effects of vertically propagating gravity waves for thermosphere general circulation models: Sensitivity study. *Journal of Geophysical Research*, 113(D19), D19106. https://doi.org/10.1029/2008JD010135
- Yiğit, E., Dhadly, M., Medvedev, A. S., Harding, B. J., Englert, C. R., Wu, Q., & Immel, T. J. (2022). Characterization of the thermospheric mean winds and circulation during solstice using ICON/MIGHTI observations. *Journal of Geophysical Research: Space Physics*, 127(11), e2022JA030851, https://doi.org/10.1029/2022JA030851
- Yiğit, E., Frey, H. U., Moldwin, M. B., Immel, T. J., & Ridley, A. J. (2016). Hemispheric differences in the response of the upper atmosphere to the August 2011 geomagnetic storm: A simulation study. *Journal of Atmospheric and Solar-Terrestrial Physics*, 141, 13–26. https://doi.org/10. 1016/j.jastp.2015.10.002
- Yiğit, E., Gann, A. L., Medvedev, A. S., Gasperini, F., Wu, Q., & Sakib, M. N. (2024). Observation of vertical coupling during a major sudden stratospheric warming by ICON and GOLD: A case study of the 2020/2021 warming event. Frontiers in Astronomy and Space Sciences, 11. https://doi.org/10.3389/fspas.2024.1384196
- Yiğit, E., Koucká Knížová, P., Georgieva, K., & Ward, W. (2016). A review of vertical coupling in the Atmosphere–Ionosphere system: Effects of waves, sudden stratospheric warmings, space weather, and of solar activity. *Journal of Atmospheric and Solar-Terrestrial Physics*, 141, 1–12. https://doi.org/10.1016/j.jastp.2016.02.011
- Yiğit, E., & Medvedev, A. S. (2009). Heating and cooling of the thermosphere by internal gravity waves. *Geophysical Research Letters*, 36(14), L14807. https://doi.org/10.1029/2009GL038507
- Yiğit, E., & Medvedev, A. S. (2015). Internal wave coupling processes in Earth's atmosphere. Advances in Space Research, 55(4), 983–1003. https://doi.org/10.1016/j.asr.2014.11.020
- Yiğit, E., & Medvedev, A. S. (2016). Role of gravity waves in vertical coupling during sudden stratospheric warmings. *Geoscience Letters*, 3(1), 27. https://doi.org/10.1186/s40562-016-0056-1
- Yiğit, E., & Medvedev, A. S. (2017). Influence of parameterized small-scale gravity waves on the migrating diurnal tide in Earth's thermosphere. Journal of Geophysical Research: Space Physics, 122(4), 4846–4864. https://doi.org/10.1002/2017JA024089
- Yiğit, E., Medvedev, A. S., & Ern, M. (2021). Effects of latitude-dependent gravity wave source variations on the middle and upper atmosphere. Frontiers in Astronomy and Space Sciences, 7, 614018. https://doi.org/10.3389/fspas.2020.614018
- Yiğit, E., & Ridley, A. J. (2011). Effects of high-latitude thermosphere heating at various scale sizes simulated by a nonhydrostatic global thermosphere–ionosphere model. *Journal of Atmospheric and Solar-Terrestrial Physics*, 73(5–6), 592–600. https://doi.org/10.1016/j.jastp. 2010.12.003
- Young, I., & Burchell, G. (1996). Hurricane generated waves as observed by satellite. Ocean Engineering, 23(8), 761–776. https://doi.org/10.1016/0029-8018(96)00001-7
- Yue, X., Schreiner, W. S., Pedatella, N., Anthes, R. A., Mannucci, A. J., Straus, P. R., & Liu, J. (2014). Space weather observations by GNSS radio occultation: From FORMOSAT-3/COSMIC to FORMOSAT-7/COSMIC-2. Space Weather, 12(11), 616–621. https://doi.org/10.1002/
- Zakharov, V. I. (2020). Experimental study of the mechanisms of the impact of large tropical cyclones on the ionosphere. In Proceedings of the 26th international symposium on atmospheric and ocean optics, atmospheric physics. Conference Name: 26th International Symposium on Atmospheric and Ocean Optics, Atmospheric Physics (Vol. 11560, p. 115607Y). Moscow, Russian Federation: SPIE. https://doi.org/10.1117/ 12.2574814
- Zambon, J. B., He, R., Warner, J. C., & Hegermiller, C. A. (2021). Impact of SST and surface waves on Hurricane Florence (2018): A coupled modeling investigation. Weather and Forecasting, 36(5), 1713–1734. https://doi.org/10.1175/waf-d-20-0171.1
- Zedler, S. E. (2009). Simulations of the ocean response to a hurricane: Nonlinear processes. *Journal of Physical Oceanography*, 39(10), 2618–2634. https://doi.org/10.1175/2009ipo4062.1
- Zhang, R., Liu, L., Ma, H., Chen, Y., & Le, H. (2022). ICON observations of equatorial ionospheric vertical E × B and field-aligned plasma drifts during the 2020–2021 SSW. *Geophysical Research Letters*, 49(16), e2022GL099238. https://doi.org/10.1029/2022GL099238
- Zhu, T., Zhang, D., & Weng, F. (2002). Impact of the advanced microwave sounding unit measurements on hurricane prediction. *Monthly Weather Review*, 130(10), 2416–2432. https://doi.org/10.1175/1520-0493(2002)130(2416:IOTAMS)2.0.CO;2
- Zolotukhina, N., Polekh, N., & Pirog, O. (2011). Variability of the ionosphere over Irkutsk at low solar activity. *Advances in Space Research*, 48(10), 1606–1612. https://doi.org/10.1016/j.asr.2011.08.006
- Zolotukhina, N., Polekh, N., Romanova, E., & Polyakova, A. (2014). Stability of the seasonal variations in diurnal and semidiurnal components of mid-latitude F2 layer parameters. Advances in Space Research, 54(3), 342–354. https://doi.org/10.1016/j.asr.2013.11.026

